SPECTRAL MEASURE COMPUTATIONS
FOR COMPOSITE MATERIALS*

N. BENJAMIN MURPHY†, ELENA CHERKAEV‡, CHRISTEL HOHENEGGER§, AND KENNETH M. GOLDEN¶

Dedicated to George Papanicolaou on the occasion of his 70th birthday.

Abstract. The analytic continuation method of homogenization theory provides Stieltjes integral representations for the effective parameters of composite media. These representations involve the spectral measures of self-adjoint random operators which depend only on the composite geometry. On finite bond lattices, these random operators are represented by random matrices and the spectral measures are given explicitly in terms of their eigenvalues and eigenvectors. Here we provide the mathematical foundation for rigorous computation of spectral measures for such composite media, and develop a numerically efficient projection method to enable such computations. This is accomplished by providing a unified formulation of the analytic continuation method which is equivalent to the original formulation and holds for finite and infinite lattices, as well as in continuum settings. We also introduce a family of bond lattices and directly compute the associated spectral measures and effective parameters. The computed spectral measures are in excellent agreement with known theoretical results. The behavior of the associated effective parameters is consistent with the symmetries and theoretical predictions of models, and the computed values fall within rigorous bounds. Some previous calculations of spectral measures have relied on finding the boundary values of the imaginary part of the effective parameter in the complex plane. Our method instead relies on direct computation of the eigenvalues and eigenvectors which enables, for example, statistical analysis of the spectral data.

Key words. Composite materials, random resistor network, percolation, homogenization, spectral measure, random matrix.

AMS subject classifications. 00B15, 47B15, 65C60, 30B40, 78A48, 80M40, 60K35.

1. Introduction

Over the years a broad range of mathematical techniques have been developed that reduce the analysis of complex composite materials with rapidly varying structures in space, to solving averaged, or *homogenized* equations involving an effective parameter. Homogenization for composite media with rapidly varying coefficients of thermal conductivity, electrical conductivity, electrical permittivity, or magnetic permeability, for example, was established by Papanicolaou and Varadhan [62] for the steady state, static case with real parameters [56]. This work was extended by Golden and Papanicolaou [33, 34] to the quasi-static frequency dependent case with complex parameters. Analysis of the effective dielectric problem for the fully frequency dependent case described by the Helmholtz equation is given in [68].

The analytic continuation method (ACM) of homogenization theory for *two-component* media in the quasi-static limit was developed by Bergman [7], Milton [53], and Golden and Papanicolaou [33], leading to Stieltjes integral representations for the effective parameters. The Golden-Papanicolaou formulation of this method is based on the spectral theorem and resolvent formulas involving random self-adjoint operators.

†Department of Mathematics, University of Utah, 155 S 1400 E RM 233, Salt Lake City, UT 84112-0090, USA (murphy@math.utah.edu).

‡Department of Mathematics, University of Utah, 155 S 1400 E RM 233, Salt Lake City, UT 84112-0090, USA (elena@math.utah.edu).

§Department of Mathematics, University of Utah, 155 S 1400 E RM 233, Salt Lake City, UT 84112-0090, USA (choheneg@math.utah.edu).

¶Department of Mathematics, University of Utah, 155 S 1400 E RM 233, Salt Lake City, UT 84112-0090, USA (golden@math.utah.edu).

This formulation demonstrated that the measures underlying these integral representations are *spectral measures* associated with the random operators, which depend only on the composite geometry. These measures contain all the information about the mixture geometry, and provide a link between microgeometry and transport. Local geometry is encoded in "geometric" resonances in the measures [46], while global connectivity is encoded by spectral gaps [58, 46] and the presence of δ-components in the measures at the spectral endpoints [58]. A remarkable feature of the method is that once the spectral measures are found for a given composite geometry, by the spectral coupling of the governing equations [13, 56, 14, 18], the effective electrical, magnetic, and thermal transport properties are *all* completely determined by these measures.

The integral representations yield rigorous *forward bounds* on the effective parameters of composites, given partial information on the microgeometry [7, 53, 33, 8, 10]. One can also use the integral representations to obtain inverse bounds, where data on the electromagnetic response of a sample, for example, is used to bound its structural parameters, such as the volume fractions of the components [51, 52, 16, 13, 17, 75, 9, 15, 21, 32], and even the separation of the inclusions in matrix particle composites [59]. Furthermore, the spectral measure can be *uniquely* reconstructed [13] when the data is given for a continuous interval of electromagnetic frequency. This, in turn, can be used to calculate other effective parameters, such as the viscoelastic modulus [15], effective thermal conductivity [14, 18], and recover the associated structural parameters [13, 17, 75, 9, 15, 21, 32]. For classes of composites which undergo a percolation transition [70, 73], the integral representations have been used to obtain detailed information regarding the critical behavior of the effective parameters in the scaling regime [30, 58]. The relationship between the effective parameters and the system energy [58] has also led to a physically consistent statistical mechanics model for two-component dielectric media which is also mathematically tractable [57].

Despite the many applications which have stemmed from the ACM, explicit analytical calculations of the effective parameters and spectral measures have been obtained for only a handful of composite microstructures. There are various numerical methods which have been used to compute the effective parameters of two-component composites. These computations may, in principle, be used to compute the corresponding spectral measures through the Stieltjes–Perron inversion theorem [43, 56]. This theorem states that the measure is recovered as a weak limit of the imaginary part of the effective parameter in the complex plane.

Highly accurate numerical computations of the effective permittivity for a class of continuum composites which have sharp corners are described in [41]. The computations are based on a multigrid recursive compressed inverse preconditioning method [42, 40, 39] developed for calculation of the effective conductivity of random checkerboards. In [20] the effective conductivity of the 2D random resistor network (RRN) was computed using an efficient algorithm that implements Y-Δ transformations of the network. In [36, 12, 35] the Fast Multipole Method was exploited to compute the electrostatic fields and the effective conductivity for two-component matrix particle composites.

In [41, 20] the spectral measures associated with the composite microstructures of interest were computed using the Stieltjes–Perron inversion theorem [43, 56]. However, the presence of δ-components or essential singularities in the measures, for example, makes it difficult to resolve details of the spectrum using this approach. To help overcome this limitation, here we develop a mathematical framework which provides a rigorous way to directly compute the spectral measures and effective parameters for finite lattice

composite microstructures, or discretizations of continuum composites. In particular, we provide a novel formulation of the ACM which is equivalent to the original formulation [33] and holds for both the finite lattice setting and the infinite settings. This analysis demonstrates that, in the finite lattice setting, the random operators underlying the integral representations of the effective parameters are represented by random matrices, and the spectral measures are determined explicitly by their eigenvalues and eigenvectors.

As a consequence, our approach provides a direct connection between the statistical behavior of spectral data of random matrices and the behavior of the effective transport processes of composites. This, in turn, has provided a direct connection between the ACM and random matrix theory, and has shown that transitions in the connectedness or percolation properties of composites are reflected in the short and long range eigenvalue correlations of the underlying random matrices [57]. Moreover, this transitional behavior provides a mechanism for the collapse of gaps in the spectral measures [57], which leads to critical behavior in the effective transport coefficients of composites [58]. This characterization of critical behavior of transport in composites by the statistical properties of eigenvalues and eigenvectors of random matrices is a key feature of the ACM and our computational approach.

2. Mathematical methods

We now formulate the effective parameter problem for random two-phase conductive media in the continuum and lattice settings, yielding Stieltjes integral representations for the effective conductivity and resistivity tensors. In Section 2.1, we review and extend the ACM for the continuum setting [33], while the lattice setting is discussed in Section 2.2. The mathematical framework underlying the *infinite* lattice setting [11, 29], reviewed in Section 2.2.1, is analogous to that of the continuum case [11], and the integral representations for the effective parameters follow with minor modifications in the theory. In Section 2.2.2, we develop a mathematical framework for the *finite* lattice setting, leading to *discrete* integral representations for the effective parameters, summarized in Theorem 2.1, which are analogous to that of the infinite, continuum and lattice cases. In order to derive the integral representations for the finite lattice setting, significant modifications must be made to the underlying mathematical framework. Toward this goal, in Section 2.2.3 we provide a novel formulation of the ACM which unifies the infinite settings and the finite lattice setting. The proof of Theorem 2.1 is given in Section 2.2.4.

2.1. Continuum setting. Consider a random two-phase conductive medium filling all of $\mathbb{R}^d$, which is determined by the probability space (Ω, P). Here, Ω is the set of all geometric realizations of our random medium, which is indexed by the parameter $\omega \in \Omega$ representing one particular geometric realization, and P is the associated probability measure. Details regarding the underlying sigma-algebra are discussed in [62]. Let $\boldsymbol{\sigma}(\vec{x}, \omega)$ and $\boldsymbol{\rho}(\vec{x}, \omega)$, $\vec{x} \in \mathbb{R}^d$, be the local complex conductivity and resistivity tensors associated with the conductive medium, which are related by $\boldsymbol{\sigma} = \boldsymbol{\rho}^{-1}$ and have components $\sigma_{jk}(\vec{x}, \omega)$ and $\rho_{jk}(\vec{x}, \omega)$, $j, k = 1, \ldots, d$, that are (spatially) stationary random fields.

A *stationary* random field, $f : \mathbb{R}^d \times \Omega \to \mathbb{C}$, is a field such that the joint distribution of $f(\vec{x}_1, \omega), \ldots, f(\vec{x}_n, \omega)$ and that of $f(\vec{x}_1 + \vec{\xi}, \omega), \ldots, f(\vec{x}_n + \vec{\xi}, \omega)$ is the same for all $\vec{\xi} \in \mathbb{R}^d$ and $n \in \mathbb{N}$ [33, 62]. More specifically, we assume that there is a group of transformations $\tau_x : \Omega \to \Omega$ and measurable functions $f'(\omega) = f(0, \omega)$ on Ω such that $f(\vec{x}, \omega) = f'(\tau_{-x} \omega)$ for all $\vec{x} \in \mathbb{R}^d$ and $\omega \in \Omega$, with $\tau_x \tau_y = \tau_{x+y}$. Moreover, we shall assume that the group is one-to-one and preserves the measure P, i.e., $P(\tau_x A) = P(A)$ for all P-measurable

sets A [33, 62]. For notational simplicity, we will not distinguish between the functions $f' : \Omega \to \mathbb{C}$ and $f : \mathbb{R}^d \times \Omega \to \mathbb{C}$, as the context of each is clear.

The group of transformations τ_x acting on Ω induces a group of operators T_x on the Hilbert space $L^2(\Omega, P)$ defined by $(T_x f)(\omega) = f(\tau_{-x}\omega)$ for all $f \in L^2(\Omega, P)$. Since τ_x is measure preserving, the operators T_x form a unitary group and therefore have closed densely defined infinitesimal generators L_i in each direction $i = 1, \ldots, d$ with domain $\mathscr{D}_i \subset L^2(\Omega, P)$ [33, 62]. Thus,

$$L_i = \frac{\partial}{\partial x_i} T_x \Big|_{x=0}, \quad i = 1, \ldots, d, \tag{2.1}$$

where x_i is the ith component of the vector $\vec{x}$ and differentiation is defined in the sense of convergence in $L^2(\Omega, P)$ for elements of $\mathscr{D}_i$ [33]. The closed subset $\mathscr{D} = \cap_{i=1}^d \mathscr{D}_i$ of $L^2(\Omega, P)$ is a Hilbert space [33] with inner product $\langle \cdot, \cdot \rangle_D$ given by $\langle f, g \rangle_D = \langle f, g \rangle_{L^2} + \sum_{i=1}^d \langle L_i f, L_i g \rangle_{L^2}$, where $\langle \cdot, \cdot \rangle_{L^2}$ is the $L^2(\Omega, P)$ inner product.

Consider the Hilbert space $\mathscr{H} = \bigotimes_{i=1}^d L^2(\Omega, P)$ with inner product $\langle \cdot, \cdot \rangle$ defined by $\langle \vec{\xi}, \vec{\zeta} \rangle = \langle \vec{\xi} \cdot \vec{\zeta} \rangle$, where $\vec{\xi} \cdot \vec{\zeta}$ denotes the dot-product on $\mathbb{C}^d$ and $\langle \cdot \rangle$ means ensemble average over Ω or, by an ergodic theorem [33], spatial average over all of $\mathbb{R}^d$. Define the Hilbert spaces [33] of "curl free" $\mathscr{H}_\times$ and "divergence free" $\mathscr{H}_\bullet$ random fields

$$\mathscr{H}_\times = \left\{ \vec{Y} \in \mathscr{H} \mid \vec{\nabla} \times \vec{Y} = 0 \text{ weakly and } \langle \vec{Y} \rangle = 0 \right\}, \tag{2.2}$$

$$\mathscr{H}_\bullet = \left\{ \vec{Y} \in \mathscr{H} \mid \vec{\nabla} \cdot \vec{Y} = 0 \text{ weakly and } \langle \vec{Y} \rangle = 0 \right\},$$

where we have used the simplified notation $\langle \vec{Y} \rangle = 0 \iff \langle Y_i \rangle = 0$ for all $i = 1, \ldots, d$, $\vec{\nabla} \cdot \vec{Y} = \sum_{i=1}^d L_i Y_i$, and $\vec{\nabla} \times \vec{Y} = 0$ means $L_i Y_j - L_j Y_i = 0$ for all $i, j = 1, \ldots, d$. Consider the following variational problems [33]. Find $\vec{E}_f \in \mathscr{H}_\times$ and $\vec{J}_f \in \mathscr{H}_\bullet$ such that

$$\langle \boldsymbol{\sigma}(\vec{E}_0 + \vec{E}_f) \cdot \vec{Y} \rangle = 0 \quad \forall \, \vec{Y} \in \mathscr{H}_\times \tag{2.3}$$

$$\langle \boldsymbol{\rho}(\vec{J}_0 + \vec{J}_f) \cdot \vec{Y} \rangle = 0 \quad \forall \, \vec{Y} \in \mathscr{H}_\bullet,$$

respectively. When the bilinear forms $\Psi(\vec{\xi}, \vec{\zeta}) = \boldsymbol{\sigma} \vec{\xi} \cdot \vec{\zeta}$ and $\Phi(\vec{\xi}, \vec{\zeta}) = \boldsymbol{\rho} \vec{\xi} \cdot \vec{\zeta}$ are bounded and coercive, these problems have unique solutions [33, 62] satisfying the quasi-static limit of Maxwell's equations [45]

$$\vec{\nabla} \times \vec{E} = 0, \quad \vec{\nabla} \cdot \vec{J} = 0, \quad \vec{J} = \boldsymbol{\sigma}\vec{E}, \quad \langle \vec{E} \rangle = \vec{E}_0, \tag{2.4}$$

$$\vec{\nabla} \times \vec{E} = 0, \quad \vec{\nabla} \cdot \vec{J} = 0, \quad \vec{E} = \boldsymbol{\rho}\vec{J}, \quad \langle \vec{J} \rangle = \vec{J}_0.$$

Here, $\vec{E}(\vec{x}, \omega) = \vec{E}_0 + \vec{E}_f(\vec{x}, \omega)$ is the random electric field, where $\vec{E}_f$ is the fluctuating field of mean zero about the (constant) average $\vec{E}_0$. Similarly, $\vec{J}(\vec{x}, \omega) = \vec{J}_0 + \vec{J}_f(\vec{x}, \omega)$ is the random current density. Moreover, the components of $\vec{E}_f$ and $\vec{J}_f$ are stationary random fields [33].

As $\vec{E}_f \in \mathscr{H}_\times$ and $\vec{J}_f \in \mathscr{H}_\bullet$, Equation (2.3) yields the energy (power) [45] constraints $\langle \vec{J} \cdot \vec{E}_f \rangle = 0$ and $\langle \vec{E} \cdot \vec{J}_f \rangle = 0$, respectively, which leads to the following reduced energy representations $\langle \vec{J} \cdot \vec{E} \rangle = \langle \vec{J} \rangle \cdot \vec{E}_0$ and $\langle \vec{E} \cdot \vec{J} \rangle = \langle \vec{E} \rangle \cdot \vec{J}_0$. The effective complex conductivity and resistivity tensors, $\boldsymbol{\sigma}^*$ and $\boldsymbol{\rho}^*$, are defined by

$$\langle \vec{J} \rangle = \boldsymbol{\sigma}^* \vec{E}_0, \tag{2.5}$$

$$\langle \vec{E} \rangle = \boldsymbol{\rho}^* \vec{J}_0.$$

Consequently, we have the following energy representations involving the effective parameters

$$\langle \vec{J} \cdot \vec{E} \rangle = \boldsymbol{\sigma}^* \vec{E}_0 \cdot \vec{E}_0, \qquad (2.6)$$
$$\langle \vec{E} \cdot \vec{J} \rangle = \boldsymbol{\rho}^* \vec{J}_0 \cdot \vec{J}_0.$$

We assume that the composite is a locally isotropic random medium so that $\sigma_{jk}(\vec{x},\omega) = \sigma(\vec{x},\omega)\delta_{jk}$ and $\rho_{jk}(\vec{x},\omega) = \rho(\vec{x},\omega)\delta_{jk}$, where δ_{jk} is the Kronecker delta and $j,k = 1,\ldots,d$. We further assume that the composite is a two-component medium, so that $\sigma(\vec{x},\omega)$ takes the *complex* values σ_1 and σ_2, and $\rho(\vec{x},\omega)$ takes the complex values $1/\sigma_1$ and $1/\sigma_2$, and satisfy [33]

$$\sigma(\vec{x},\omega) = \sigma_1 \chi_1(\vec{x},\omega) + \sigma_2 \chi_2(\vec{x},\omega), \qquad (2.7)$$
$$\rho(\vec{x},\omega) = \sigma_1^{-1} \chi_1(\vec{x},\omega) + \sigma_2^{-1} \chi_2(\vec{x},\omega).$$

Here, $\chi_i(\vec{x},\omega)$ is the characteristic function of medium $i = 1,2$, which equals one for all $\omega \in \Omega$ having medium i at $\vec{x}$ and zero otherwise, with $\chi_1 = 1 - \chi_2$. For simplicity, we focus on one component, $\sigma_{jk}^* = [\boldsymbol{\sigma}^*]_{jk}$ and $\rho_{jk}^* = [\boldsymbol{\rho}^*]_{jk}$, of these symmetric tensors, for some $j,k = 1,\ldots,d$.

Due to the homogeneity of these functions, e.g., $\sigma_{jk}^*(a\sigma_1, a\sigma_2) = a\sigma_{jk}^*(\sigma_1,\sigma_2)$ for any complex number a, they depend only on the ratio $h = \sigma_1/\sigma_2$, and we define the tensor-valued functions $\mathbf{m}(h) = \boldsymbol{\sigma}^*/\sigma_2$, $\mathbf{w}(z) = \boldsymbol{\sigma}^*/\sigma_1$, $\tilde{\mathbf{m}}(h) = \sigma_1 \boldsymbol{\rho}^*$, and $\tilde{\mathbf{w}}(z) = \sigma_2 \boldsymbol{\rho}^*$ with components

$$m_{jk}(h) = \sigma_{jk}^*/\sigma_2, \quad w_{jk}(z) = \sigma_{jk}^*/\sigma_1, \qquad (2.8)$$
$$\tilde{m}_{jk}(h) = \sigma_1 \rho_{jk}^*, \quad \tilde{w}_{jk}(z) = \sigma_2 \rho_{jk}^*,$$

where $z = 1/h$. The dimensionless functions $m_{jk}(h)$ and $\tilde{m}_{jk}(h)$ are analytic off the negative real axis in the h-plane, while $w_{jk}(z)$ and $\tilde{w}_{jk}(z)$ are analytic off the negative real axis in the z-plane [33]. Each take the corresponding upper half plane to the upper half plane and are therefore examples of Herglotz functions [22, 33].

A key step in the ACM is obtaining Stieltjes integral representations for $\boldsymbol{\sigma}^*$ and $\boldsymbol{\rho}^*$. These follow from resolvent representations for the electric field $\vec{E}$ [33] and current density $\vec{J}$ [58]

$$\vec{E} = s(sI - \Gamma\chi_1)^{-1}\vec{E}_0 = t(tI - \Gamma\chi_2)^{-1}\vec{E}_0, \quad s \in \mathbb{C}\backslash[0,1], \qquad (2.9)$$
$$\vec{J} = t(tI - \Upsilon\chi_1)^{-1}\vec{J}_0 = s(sI - \Upsilon\chi_2)^{-1}\vec{J}_0, \quad t \in \mathbb{C}\backslash[0,1],$$

where I is the identity operator on $\mathbb{R}^d$ and we have defined the complex variables $s = 1/(1-h)$ and $t = 1/(1-z) = 1-s$. The operator $\Gamma = \vec{\nabla}(\Delta^{-1})\vec{\nabla}\cdot$ is based on convolution with the free-space Green's function for the Laplacian $\Delta = \vec{\nabla}\cdot\vec{\nabla} = \nabla^2$, and the operator $\Upsilon = \vec{\nabla}\times(\vec{\nabla}\times\vec{\nabla}\times)^{-1}\vec{\nabla}\times$ involves the vector Laplacian $\boldsymbol{\Delta} = -\vec{\nabla}\times\vec{\nabla}\times + \vec{\nabla}\vec{\nabla}\cdot$ when $d = 3$ [33, 58]. These (non-random) integro-differential operators and the origin of the resolvent equations in (2.9) are discussed in more detail below.

If the current density $\vec{J}(\vec{x},\omega)$ and the electric field $\vec{E}(\vec{x},\omega)$ are sufficiently smooth for all $\vec{x} \in \mathbb{R}^d$ when $\omega \in \Omega$, Equation (2.9) is obtained as follows. The operator Δ^{-1} is well defined in terms of convolution with respect to the free-space Green's function of the Laplacian Δ [33, 26, 69]. Similarly, the inverse $\boldsymbol{\Delta}^{-1}$ of the vector Laplacian $\boldsymbol{\Delta}$ is defined in terms of component-wise convolution with respect to the free-space Green's function of the Laplacian.

Applying the integro-differential operator $\vec{\nabla}(\Delta^{-1})$ to the formula $\vec{\nabla}\cdot\vec{J}=0$ in Equation (2.4) yields $\Gamma\vec{J}=0$, where $\Gamma=\vec{\nabla}(\Delta^{-1})\vec{\nabla}\cdot$ is an orthogonal projection [33] from $\mathscr{H}$ onto the Hilbert space $\mathscr{H}_\times$ of curl-free random fields, $\Gamma:\mathscr{H}\mapsto\mathscr{H}_\times$. More specifically, for every sufficiently smooth $\vec{\zeta}\in\mathscr{H}_\times$ there exists [45] a scalar potential φ which is unique up to a constant such that $\vec{\zeta}=\vec{\nabla}\varphi$. Consequently, since $\Delta=\vec{\nabla}\cdot\vec{\nabla}$, it is clear that $\Gamma\vec{\zeta}=\vec{\zeta}$ for all such $\vec{\zeta}\in\mathscr{H}_\times$ [26, 69].

For simplicity, we discuss only the analogous properties of divergence free vector fields and the projection operator $\Upsilon=\vec{\nabla}\times(\vec{\nabla}\times\vec{\nabla}\times)^{-1}\vec{\nabla}\times$, restricting our attention to $d=3$ to avoid a more involved discussion regarding differential forms [19]. Applying the integro-differential operator $-\vec{\nabla}\times(\Delta^{-1})$ to the formula $\vec{\nabla}\times\vec{E}=0$ in Equation (2.4) yields $\Upsilon\vec{E}=0$. Here, $\Upsilon=-\vec{\nabla}\times(\Delta^{-1})\vec{\nabla}\times$ is an orthogonal projection from $\mathscr{H}$ onto the Hilbert space $\mathscr{H}_\bullet$ of divergence-free random fields, $\Upsilon:\mathscr{H}\mapsto\mathscr{H}_\bullet$, of transverse gauge [58]. This can be seen as follows. For every sufficiently smooth $\vec{\zeta}\in\mathscr{H}_\bullet$ we have the representation $\vec{\zeta}=\vec{\nabla}\times(\vec{A}+\vec{C})$, where $\vec{A}$ is a vector potential associated with $\vec{\zeta}$ and the arbitrary vector field $\vec{C}$ satisfies $\vec{\nabla}\times\vec{C}=0$ [45]. Without loss of generality, the vector field $\vec{C}$ can be chosen so that $\vec{A}$ satisfies $\vec{\nabla}\cdot\vec{A}=0$ [45]. Hence, $\vec{\nabla}\times\vec{\zeta}=\vec{\nabla}\times\vec{\nabla}\times\vec{A}=\vec{\nabla}(\vec{\nabla}\cdot\vec{A})-\Delta\vec{A}=-\Delta\vec{A}$. The vector field $\vec{C}$ chosen in this manner gives the transverse *gauge* of $\vec{\zeta}$ [45]. Choosing the members of $\mathscr{H}_\bullet$ to have transverse gauge, the action of $\vec{\nabla}\times\vec{\nabla}\times$ on $\mathscr{H}_\bullet$ is given by that of $-\Delta$. Therefore, the action of Υ on $\mathscr{H}_\bullet$ is given by that of

$$\Upsilon=\vec{\nabla}\times(\vec{\nabla}\times\vec{\nabla}\times)^{-1}\vec{\nabla}\times=-\vec{\nabla}\times(\Delta^{-1})\vec{\nabla}\times, \tag{2.10}$$

and it is clear from the above discussion that $\Upsilon\vec{\zeta}=\vec{\zeta}$ for all such $\vec{\zeta}\in\mathscr{H}_\bullet$ [26, 69]. In general, the differential operators $\vec{\nabla}$, $\vec{\nabla}\cdot$ and $\vec{\nabla}\times$ are interpreted in a weak sense in terms of the operators L_i in (2.1) [33], and the equalities $\Gamma\vec{\zeta}=\vec{\zeta}$ and $\Upsilon\vec{\zeta}=\vec{\zeta}$ displayed above are in the $L^2(\Omega,P)$ sense [26, 69].

We now derive the resolvent formulas in Equation (2.9). Write σ and ρ in Equation (2.7) as $\sigma=\sigma_2(1-\chi_1/s)=\sigma_1(1-\chi_2/t)$ and $\rho=(1-\chi_2/s)/\sigma_1=(1-\chi_1/t)/\sigma_2$. Recall that $\vec{E}=\vec{E}_0+\vec{E}_f$, where $\vec{E}_0$ is a *constant* field and $\vec{E}_f\in\mathscr{H}_\times$, so that $\Gamma\vec{E}=\vec{E}_f$ and similarly $\Upsilon\vec{J}=\vec{J}_f$ in $L^2(\Omega,P)$. Consequently, from $\Gamma\vec{J}=0$ and $\Upsilon\vec{E}=0$ we have the following formulas which are equivalent to that in (2.9):

$$\vec{E}_f=\frac{1}{s}\Gamma\chi_1\vec{E}=\frac{1}{t}\Gamma\chi_2\vec{E}, \tag{2.11}$$
$$\vec{J}_f=\frac{1}{s}\Upsilon\chi_2\vec{J}=\frac{1}{t}\Upsilon\chi_1\vec{J}.$$

On the Hilbert space $\mathscr{H}_\times$, the operators Γ and χ_i, $i=1,2$, act as projectors [33]. Therefore $M_i=\chi_i\Gamma\chi_i$, $i=1,2$, are compositions of projection operators on $\mathscr{H}_\times$, and are consequently positive definite and bounded by 1 in the underlying operator norm [64, 72]. They are self-adjoint with respect to the $\mathscr{H}$-inner-product $\langle\cdot,\cdot\rangle$ [33]. Therefore, on the Hilbert space $\mathscr{H}_\times$ with weight χ_1 in the inner-product, $\langle\cdot,\cdot\rangle_1=\langle\chi_1\cdot,\cdot\rangle$ for example, $\Gamma\chi_1$ is a bounded linear self-adjoint operator with spectrum contained in the interval $[0,1]$ [33, 63, 72]. Hence, the resolvent operator $(sI-\Gamma\chi_1)^{-1}$ in (2.9) is also a bounded linear self-adjoint operator with respect to the same inner-product for $s\in\mathbb{C}\backslash[0,1]$ [72]. Similarly, $(tI-\Upsilon\chi_1)^{-1}$ in (2.9) is a bounded linear self-adjoint operator on $\mathscr{H}_\bullet$ with respect to the inner-product $\langle\cdot,\cdot\rangle_1$ for $t\in\mathbb{C}\backslash[0,1]$.

To obtain integral representations for $\boldsymbol{\sigma}^*$ and $\boldsymbol{\rho}^*$, it is more convenient to consider the functions $F_{jk}(s)=\delta_{jk}-m_{jk}(h)$ and $E_{jk}(s)=\delta_{jk}-\tilde{m}_{jk}(h)$ which are analytic off $[0,1]$

in the s-plane, and $G_{jk}(t) = \delta_{jk} - w_{jk}(z)$ and $H_{jk}(t) = \delta_{jk} - \tilde{w}_{jk}(z)$ which are analytic off $[0,1]$ in the t-plane [33]. For the formulation of the effective parameter problem involving $\mathscr{H}_\times$ and $\boldsymbol{\sigma}^*$, define the coordinate system so that in (2.5) the constant vector $\vec{E}_0$ is given by $\vec{E}_0 = E_0 \vec{e}_j$, where $\vec{e}_j$ is the standard basis vector on $\mathbb{R}^d$ in the jth direction for some $j = 1, \ldots, d$. In the other formulation involving $\mathscr{H}_\bullet$ and $\boldsymbol{\rho}^*$, define $\vec{J}_0 = J_0 \vec{e}_j$. Equations (2.5) and (2.9) and the spectral theorem for bounded linear self-adjoint operators [63, 72] then yield the following Stieltjes integral representations [33, 6, 8, 58] for the effective parameters σ_{jk}^* and ρ_{jk}^* (see sections 2.2.3 and A.1 for more details):

$$m_{jk}(h) = \delta_{jk} - F_{jk}(s), \qquad F_{jk}(s) = \langle \chi_1 (sI - \Gamma\chi_1)^{-1} \vec{e}_j \cdot \vec{e}_k \rangle = \int_0^1 \frac{\mathrm{d}\mu_{jk}(\lambda)}{s - \lambda}, \qquad (2.12)$$

$$w_{jk}(z) = \delta_{jk} - G_{jk}(t), \qquad G_{jk}(t) = \langle \chi_2 (tI - \Gamma\chi_2)^{-1} \vec{e}_j \cdot \vec{e}_k \rangle = \int_0^1 \frac{\mathrm{d}\alpha_{jk}(\lambda)}{t - \lambda},$$

$$\tilde{m}_{jk}(h) = \delta_{jk} - E_{jk}(s), \qquad E_{jk}(s) = \langle \chi_2 (sI - \Upsilon\chi_2)^{-1} \vec{e}_j \cdot \vec{e}_k \rangle = \int_0^1 \frac{\mathrm{d}\eta_{jk}(\lambda)}{s - \lambda},$$

$$\tilde{w}_{jk}(z) = \delta_{jk} - H_{jk}(t), \qquad H_{jk}(t) = \langle \chi_1 (tI - \Upsilon\chi_1)^{-1} \vec{e}_j \cdot \vec{e}_k \rangle = \int_0^1 \frac{\mathrm{d}\kappa_{jk}(\lambda)}{t - \lambda}.$$

Equation (2.12) displays Stieltjes integrals involving *spectral measures of random operators*. More specifically, $\mathrm{d}\mu_{jk}(\lambda)$ and $\mathrm{d}\alpha_{jk}(\lambda)$ are spectral measures associated with the random operators $\chi_1\Gamma\chi_1$ and $\chi_2\Gamma\chi_2$, while $\mathrm{d}\eta_{jk}(\lambda)$ and $\mathrm{d}\kappa_{jk}(\lambda)$ are spectral measures associated with the random operators $\chi_2\Upsilon\chi_2$ and $\chi_1\Upsilon\chi_1$, respectively. In particular, there is a one-to-one correspondence between the bounded linear self-adjoint operator $\chi_1\Gamma\chi_1$ on $\mathscr{H}_\times$, for example, and a family of projection operators $Q(\lambda)$, parameterized by $\lambda \in [0,1]$, which satisfies $\lim_{\lambda \to 0} Q(\lambda) = 0$ and $\lim_{\lambda \to 1} Q(\lambda) = I$, where 0 and I are the null and identity operators on $\mathscr{H}_\times$, respectively [72]. The strictly increasing function $\mu_{jk}(\lambda) = \langle Q(\lambda)\vec{e}_j, \vec{e}_k \rangle_1$ of the spectral variable λ is of bounded variation [72]. The spectral measure $\mathrm{d}\mu_{jk}(\lambda)$ is a *Stieltjes measure* [27] associated with the function $\mu_{jk}(\lambda)$ [72] (see Section A.1 for more details). For notational simplicity, we will often refer to the measure μ_{jk}, not to be confused with the function $\mu_{jk}(\lambda)$.

By the Stieltjes–Perron inversion theorem [43, 56], the matrix valued function $\boldsymbol{\mu}(\lambda)$ with components $\mu_{jk}(\lambda)$, $j,k = 1, \ldots, d$, for example, is given by the weak limit $\boldsymbol{\mu}(\lambda) = -(1/\pi)\lim_{\varepsilon \downarrow 0} \mathrm{Im}(\mathbf{F}(\lambda + \imath\varepsilon))$, i.e.,

$$\int_0^1 \xi(\lambda)\,\mathrm{d}\boldsymbol{\mu}(\lambda) = -\frac{1}{\pi}\lim_{\varepsilon \downarrow 0} \int_0^1 \xi(\lambda)\,\mathrm{Im}(\mathbf{F}(\lambda + \imath\varepsilon))\,\mathrm{d}\lambda, \qquad (2.13)$$

for all smooth test functions $\xi(\lambda)$, where $[\mathbf{F}(s)]_{jk} = F_{jk}(s)$ and $[\mathrm{d}\boldsymbol{\mu}(\lambda)]_{jk} = \mathrm{d}\mu_{jk}(\lambda)$. From Equation (2.13) and the identities $m_{jk}(h) = h w_{jk}(z)$ and $\tilde{m}_{jk}(h) = h \tilde{w}_{jk}(z)$, which follow from Equation (2.8), it has been shown [58] that the functions $\mu_{jk}(\lambda)$ and $\alpha_{jk}(\lambda)$, and the functions $\eta_{jk}(\lambda)$ and $\kappa_{jk}(\lambda)$ are related by

$$\lambda\mu_{jk}(\lambda) = (1 - \lambda)\alpha_{jk}(1 - \lambda) + \lambda\varrho(\lambda), \qquad \mathrm{d}\varrho(\lambda) = w_{jk}(0)\delta_0(\mathrm{d}\lambda) + m_{jk}(0)(\lambda - 1)\delta_1(\mathrm{d}\lambda),$$

$$\lambda\kappa_{jk}(\lambda) = (1 - \lambda)\eta_{jk}(1 - \lambda) + \lambda\tilde{\varrho}(\lambda), \qquad \mathrm{d}\tilde{\varrho}(\lambda) = \tilde{m}_{jk}(0)\delta_0(\mathrm{d}\lambda) + \tilde{w}_{jk}(0)(\lambda - 1)\delta_1(\mathrm{d}\lambda).$$
$$(2.14)$$

Here, $m_{jk}(0) = m_{jk}(h)|_{h=0}$ and $w_{jk}(0) = w_{jk}(z)|_{z=0}$, for example, and $\delta_a(\mathrm{d}\lambda)$ is the delta measure concentrated at $\lambda = a$.

Equations (2.12) and (2.14) demonstrate the many symmetries between the functions $m_{jk}(h)$, $w_{jk}(z)$, $\tilde{m}_{jk}(h)$, and $\tilde{w}_{jk}(z)$, and the respective measures μ_{jk}, α_{jk}, η_{jk},

and κ_{jk}. Because of these symmetries, for simplicity, we will focus on $m_{jk}(h)$ and μ_{jk}, and will reintroduce the other functions and measures where appropriate.

A key feature of equations (2.5), (2.8), and (2.12) is that the parameter information in h and E_0 is *separated* from the geometry of the composite, which is encoded in the spectral measure μ_{jk} via its moments μ_{jk}^n [33, 11],

$$\mu_{jk}^n = \int_0^1 \lambda^n \mathrm{d}\mu_{jk}(\lambda) = \langle \chi_1[\Gamma\chi_1]^n \vec{e}_j \cdot \vec{e}_k \rangle, \quad n=0,1,2,\ldots, \tag{2.15}$$

where the second equality follows from the spectral theorem displayed in Equation (A.2). Since χ_1 operates pointwise on $\mathbb{R}^d$ and the constant vectors $\vec{e}_j$, $j=1,\ldots,d$, are non-random, we see from Equation (2.15) that the mass μ_{jk}^0 of the measure μ_{jk} is given by

$$\mu_{jk}^0 = p_1 \delta_{jk}, \tag{2.16}$$

where $p_1 = \langle \chi_1 \rangle$ is the volume fraction of material component one. This demonstrates that the diagonal components μ_{kk}, $k=1,\ldots,d$, of $\boldsymbol{\mu}$ are *positive measures*, while the off-diagonal components μ_{jk}, $j \neq k=1,\ldots,d$, have zero mass and are consequently *signed measures* [27, 64]. The positivity of the measure μ_{kk} also follows from the fact that $Q(\lambda)$ is a *self-adjoint projector* on $\mathscr{H}_\times$ so that $\langle Q(\lambda)\vec{e}_k \cdot \vec{e}_k \rangle_1 = \langle Q(\lambda)\vec{e}_k \cdot Q(\lambda)\vec{e}_k \rangle_1 = \|Q(\lambda)\vec{e}_k\|_1^2$ is a strictly increasing function of λ [72]. Therefore, the Stieltjes measure of an arbitrary set $A \subseteq [0,1]$ is positive [27],

$$\mu_{kk}(A) = \int_A d\mu_{kk}(\lambda) = \int_A d\|Q(\lambda)\vec{e}_k\|_1^2 \geq 0, \tag{2.17}$$

where $\|\cdot\|_1$ denotes the norm induced by the inner-product $\langle \cdot,\cdot \rangle_1$ [27, 64].

The higher order moments μ_{jk}^n, $n=1,2,3,\ldots$, in principle, may be found using a perturbation expansion of $F_{jk}(s)$ about a homogeneous medium, $(\sigma_1 = \sigma_2,\ s=\infty)$ [33, 11]. In particular $\mu_{jk}^0 = p_1 \delta_{jk}$, generically, and $\mu_{jk}^1 = (p_1 p_2/d)\delta_{jk}$ for a statistically isotropic random medium [33, 31, 11], where $p_2 = 1 - p_1 = \langle \chi_2 \rangle$ is the volume fraction of material component 2. In the case of a square bond lattice, which is an example of an infinitely interchangeable random medium [11], $\mu_{kk}^2 = p_1 p_2(1 + (d-2)p_1)/d^2$ for any dimension d and $\mu_{kk}^3 = p_1 p_2(1 + p_1 - p_1^2)/8$ for $d=2$. In general, the moments μ_{jk}^n depend on the $(n+1)$-point correlation functions of the random medium [33, 11].

A principal application of the ACM is to derive *forward bounds* on the diagonal components σ_{kk}^* of the tensor $\boldsymbol{\sigma}^*$, $k=1,\ldots,d$, given partial information on the microgeometry [7, 53, 33, 8]. This information may be given in terms of the moments μ_{kk}^n, $n=0,1,2,\ldots$, of the measure μ_{kk} [55, 33]. Given this information, the bounds on σ_{kk}^* follow from the special structure of $F_{kk}(s)$ in (2.12). More specifically, it is a *linear* functional of the *positive* measure μ_{kk}. The bounds are obtained by fixing the contrast parameter s, varying over an admissible set of measures μ_{kk} (or geometries) which is determined by the known information regarding the two-component composite. Knowledge of the moments μ_{kk}^n for $n=1,\ldots,J$ confines σ_{kk}^* to a region of the complex plane which is bounded by arcs of circles, and the region becomes progressively smaller as more moments are known [55, 28]. When all the moments are known, the measure μ_{kk} is uniquely determined [1], hence σ_{kk}^* is explicitly known. The bounding procedure is reviewed in Section 2.3.

We conclude this section with a discussion regarding some consequences of the energy constraints $\langle \vec{J} \cdot \vec{E}_f \rangle = 0 = \langle \vec{E} \cdot \vec{J}_f \rangle$, which follow from Equation (2.3), and are at

the heart of the existence and uniqueness of solutions to the systems of equations in (2.4). We first note that the formulas $\Gamma\vec{E}=\vec{E}_f$ and $\Upsilon\vec{J}=\vec{J}_f$ are sufficient conditions for these constraints. The sufficiency of these conditions can be seen by writing $\sigma=\sigma_2(1-\chi_1/s)$ and $\rho=(1-\chi_1/t)/\sigma_2$ in $\vec{J}=\sigma\vec{E}$ and $\vec{E}=\rho\vec{J}$, respectively, to obtain

$$\langle\vec{J}\cdot\vec{E}_f\rangle=\sigma_2(\langle\vec{E}\cdot\vec{E}_f\rangle-\langle\chi_1\vec{E}\cdot\vec{E}_f\rangle/s),\quad\langle\vec{E}\cdot\vec{J}_f\rangle=(\langle\vec{J}\cdot\vec{J}_f\rangle-\langle\chi_1\vec{J}\cdot\vec{J}_f\rangle/t)/\sigma_2,\quad(2.18)$$

for $s\neq0$ ($h\neq\infty$) and $t\neq0$ ($h\neq0$). Now, if we have $\Gamma\vec{E}=\vec{E}_f$ then $\vec{\nabla}\cdot\vec{J}=0$ yields the formula $\vec{E}_f=\Gamma\chi_1\vec{E}/s$ of Equation (2.11). Therefore, as Γ is a self-adjoint operator on $\mathscr{H}$ [33, 69, 72, 26], we have

$$\langle\chi_1\vec{E}\cdot\vec{E}_f\rangle=\langle\chi_1\vec{E}\cdot\Gamma\vec{E}\rangle=\langle\Gamma\chi_1\vec{E}\cdot\vec{E}\rangle=s\langle\vec{E}_f\cdot\vec{E}\rangle.\tag{2.19}$$

Consequently, from Equation (2.18) we have $\langle\vec{J}\cdot\vec{E}_f\rangle=0$ for $s\neq0$. The argument involving the operator Υ and the vector field $\vec{J}_f$ is analogous.

We see from Equation (2.18) that the energy constraints are equivalent to the following "field representations" for the contrast parameters s and t:

$$\langle\chi_1\vec{E}\cdot\vec{E}_f\rangle/\langle\vec{E}\cdot\vec{E}_f\rangle=s=1-t=1-\langle\chi_1\vec{J}\cdot\vec{J}_f\rangle/\langle\vec{J}\cdot\vec{J}_f\rangle,\tag{2.20}$$

when $\langle\vec{E}\cdot\vec{E}_f\rangle\neq0$ (if and only if $\langle\chi_1\vec{E}\cdot\vec{E}_f\rangle\neq0$ when $s\neq0$ from (2.19)), for example. Moreover, the energy constraints provide the limiting behavior of the ratio $\mathcal{R}(h)=\langle\vec{E}\cdot\vec{E}_f\rangle/\langle\chi_1\vec{E}\cdot\vec{E}_f\rangle=1/s$, for example,

$$\lim_{h\to0}\mathcal{R}(h)=1,\quad\lim_{h\to1}\mathcal{R}(h)=0,\quad\lim_{h\to+\infty}\mathcal{R}(h)=-\infty,\tag{2.21}$$

which is otherwise a very complicated object in the absence of these energy constraints. We also note that Equation (2.20) provides a relationship between the members $\vec{E}_f$ and $\vec{J}_f$ of the Hilbert spaces $\mathscr{H}_\times$ and $\mathscr{H}_\bullet$, respectively.

The energy constraints also lead to detailed decompositions of the system energy $\langle\vec{J}\cdot\vec{E}\rangle$ in terms of Stieltjes integrals involving the measures μ_{jj}, α_{jj}, η_{jj}, and κ_{jj} [58, 57]. For example, $\langle\vec{J}\cdot\vec{E}_f\rangle=0$, $\vec{E}=\vec{E}_0+\vec{E}_f$, $\vec{E}_0=E_0\vec{e}_j$, $\langle\vec{E}_f\rangle=0$, and $\sigma=\sigma_2(1-\chi_1/s)$ together imply that $0=\langle\sigma\vec{E}\cdot\vec{E}_f\rangle=\langle\sigma_2(1-\chi_1/s)(\vec{E}_0\cdot\vec{E}_f+E_f^2)\rangle=\sigma_2\left[\langle E_f^2\rangle-\langle\chi_1\vec{E}\cdot\vec{E}_f\rangle/s\right]$, where $E_f^2=|\vec{E}_f|^2$. Equation (2.9) and the spectral theorem displayed in Equation (A.2) then yield [58]

$$\frac{\langle E_f^2\rangle}{E_0^2}=\int_0^1\frac{\lambda\,\mathrm{d}\mu_{jj}(\lambda)}{|s-\lambda|^2}=\int_0^1\frac{\lambda\,\mathrm{d}\alpha_{jj}(\lambda)}{|t-\lambda|^2}.\tag{2.22}$$

Equation (2.22), in turn, leads to Stieltjes integral representations of all such energy components involving these measures [57]. Analogous energy decompositions involving $\vec{J}_f$ and the measures η_{jj} and κ_{jj} similarly follow. In [57] this energy decomposition has lead to a physically transparent statistical mechanics model of two-phase dielectric media.

2.2. Lattice setting. In this section, we formulate the effective parameter problem for the infinite and finite, two-component bond lattice on $\mathbb{Z}^d$ (formulations for other lattice topologies are analogous). The infinite bond lattice, reviewed in Section 2.2.1, is a special case of the stationary random medium considered in Section 2.1. In Section 2.2.2, we develop a mathematical framework for the ACM in the finite lattice setting, a key theoretical contribution of this work.

2.2.1. Infinite lattice setting. Consider a two-component bond lattice on all of $\mathbb{Z}^d$ determined by the probability space (Ω, P), and let $\boldsymbol{\sigma}(\vec{x}, \omega)$ be the local complex conductivity tensor with components $\sigma_{jk}(\vec{x}, \omega) = \sigma^j(\vec{x}, \omega)\delta_{jk}$, $j, k = 1, \ldots, d$. Here, $\sigma^j(\vec{x}, \omega)$ is the conductivity of the bond emanating from $\vec{x} \in \mathbb{Z}^d$ in the positive j^{th} direction for $\omega \in \Omega$, which is a stationary random field that takes the *complex* values σ_1 and σ_2 with probabilities p_1 and $p_2 = 1 - p_1$, respectively [29, 11]. The configuration space $\Omega = \{\sigma_1, \sigma_2\}^{d\mathbb{Z}^d}$ represents the set of all realizations of the random medium and the probability measure P is compatible with stationarity. Analogous to Equation (2.7), the local conductivity $\sigma^j(\vec{x}, \omega)$ of the two-phase random medium takes the form [29]

$$\sigma^j(\vec{x}, \omega) = \sigma_1 \chi_1^j(\vec{x}, \omega) + \sigma_2 \chi_2^j(\vec{x}, \omega), \quad j = 1, \ldots, d. \tag{2.23}$$

Here, $\chi_i^j(\vec{x}, \omega)$ is the characteristic function of medium $i = 1, 2$, which equals one for all realizations $\omega \in \Omega$ having medium i in the jth positive bond at $\vec{x}$, and equals zero otherwise.

In this lattice setting, the differential operators $\vec{\nabla} \times$ and $\vec{\nabla} \cdot$ in Equation (2.4) are given [29, 11] in terms of forward and backward difference operators D_j^+ and D_j^-, respectively, where

$$D_j^+ = T_j^+ - I, \quad D_j^- = I - T_j^-, \quad j = 1, \ldots, d. \tag{2.24}$$

Here, I is the identity operator on $\mathbb{Z}^d$, and $T_j^+ = T_{+e_j}$ and $T_j^- = T_{-e_j}$ are the generators (through composition) of the unitary group T_x acting on $L^2(\Omega, P)$ defined by $(T_x f)(0, \omega) = f(\vec{x}, \omega)$, for any $f \in L^2(\Omega, P)$ which is a stationary random field [29]. Define $\mathscr{H} = \bigotimes_{i=1}^d L^2(\Omega, P)$ and let $\vec{E}, \vec{J} \in \mathscr{H}$ be the random electric field and current density, respectively, where $\vec{E}(\vec{x}, \omega) = (E^1(\vec{x}, \omega), \ldots, E^d(\vec{x}, \omega))$ and $E^j(\vec{x}, \omega)$ is the electric field in the bond emanating from $\vec{x}$ in the positive j^{th} direction, and similarly for $\vec{J}(\vec{x}, \omega)$.

As in Section 2.1 we write $\vec{E} = \vec{E}_0 + \vec{E}_f$, where $\vec{E}_f$ is the fluctuating field of mean zero about the (constant) average $\vec{E}_0$. The variational problem in (2.3) for this lattice setting has a unique solution satisfying Kirchhoff's circuit laws [33, 11],

$$D_i^+ E^j - D_j^+ E^i = 0, \quad \sum_{k=1}^d D_k^- J^k = 0, \quad J^i = \sigma^i E^i, \quad \langle \vec{E} \rangle = \vec{E}_0, \tag{2.25}$$

where $i, j = 1, \ldots, d$ and the components $E^i(\vec{x}, \omega)$ and $J^i(\vec{x}, \omega)$ of $\vec{E}(\vec{x}, \omega)$ and $\vec{J}(\vec{x}, \omega)$ are stationary random fields. Equation (2.25) is a direct analogue of Equation (2.4) when written in component form [33]. The effective complex conductivity tensor $\boldsymbol{\sigma}^*$ is defined by $\langle \vec{J} \rangle = \boldsymbol{\sigma}^* \vec{E}_0$, and has components $\sigma_{jk}^* = \sigma_2 m_{jk}(h)$, $j, k = 1, \ldots, d$, where $h = \sigma_1/\sigma_2$. The representation formula for $m_{jk}(h)$ in (2.12) still holds in this infinite lattice setting, with Γ in (2.9) now given by

$$\Gamma = \nabla^+ (\Delta^{-1}) \nabla^-, \quad \nabla^\pm = (D_1^\pm, \ldots, D_d^\pm), \tag{2.26}$$

where Δ^{-1} is based on discrete convolution with the lattice Green's function for the Laplacian $\Delta = \nabla^- \nabla^+$ [11]. The formulation of the ACM for the effective resistivity tensor $\boldsymbol{\rho}^*$ in the infinite lattice setting is analogous to that for $\boldsymbol{\sigma}^*$ given here. In Section 2.2.2 we discuss in detail the operator Υ underlying the integral representations for $\boldsymbol{\rho}^*$ in the lattice setting.

2.2.2. Finite lattice setting.   Consider a finite, two-component bond lattice on $\mathbb{Z}_L^d \subset \mathbb{Z}^d$ determined by the probability space (Ω, P), where

$$\mathbb{Z}_L^d = \{\vec{x} \in \mathbb{Z}^d \mid 1 \leq x_i \leq L, \ i = 1, \ldots, d\}, \tag{2.27}$$

$L \in \mathbb{N}$, $L \geq 2$, and x_i is the ith component of the vector $\vec{x}$. Let $\boldsymbol{\sigma}(\vec{x}, \omega)$ be the local complex conductivity tensor with components $\sigma_{jk}(\vec{x}, \omega) = \sigma^j(\vec{x}, \omega)\delta_{jk}$, $j, k = 1, \ldots, d$, where $\sigma^j(\vec{x}, \omega)$ is defined in Equation (2.23) for $\vec{x} \in \mathbb{Z}_L^d$ and $\omega \in \Omega$. The configuration space $\Omega = \{\sigma_1, \sigma_2\}^{d\mathbb{Z}_L^d}$ represents the set of all 2^N realizations of the finite random bond lattice, where $N = dL^d$ and P is the associated (discrete) probability measure. Define $\mathscr{H} = \bigotimes_{i=1}^d L^2(\Omega, P)$ and let $\vec{E}, \vec{J} \in \mathscr{H}$ be the random electric field and current density, respectively, which satisfy Kirchhoff's circuit laws in (2.25) with appropriate boundary conditions. Analogous to Equation (2.5), the effective complex conductivity tensor $\boldsymbol{\sigma}^*$ is defined by $\langle \vec{J} \rangle = \boldsymbol{\sigma}^* \vec{E}_0$, and has components $\sigma_{jk}^* = \sigma_2 m_{jk}(h)$, where $\vec{E}_0 = \langle \vec{E} \rangle$ and $\langle \cdot \rangle$ denotes ensemble average over Ω. In a similar way we define the functions $\sigma_{jk}^* = \sigma_1 w_{jk}(z)$ and $\rho_{jk}^* = \tilde{m}_{jk}(h)/\sigma_1 = \tilde{w}_{jk}(z)/\sigma_2$ introduced in Equation (2.8).

In this section, we obtain discrete versions of the integral representations for $m_{jk}(h)$ and $\tilde{w}_{jk}(z)$ displayed in Equation (2.12) for this finite bond lattice setting, involving spectral measures μ_{jk} and κ_{jk} associated with real-symmetric random matrices. The formulation involving the functions $\tilde{m}_{jk}(h)$ and $w_{jk}(z)$ in (2.12) is analogous. Toward this goal, we define a bijective mapping Θ from the d-dimensional set $\mathbb{Z}_L^d$ onto the one dimensional set $\mathbb{N}_L \subset \mathbb{N}$, $\Theta : \mathbb{Z}_L^d \to \mathbb{N}_L$, given by

$$\mathbb{N}_L = \{i \in \mathbb{N} \mid i \leq dL^d\}, \qquad \Theta(\vec{x}) = x_1 + \sum_{k=2}^d (x_k - 1)L^{k-1}. \tag{2.28}$$

Under the bijection Θ the components $E^j(\vec{x}, \omega)$, $j = 1, \ldots, d$, of the random electric field $\vec{E}(\vec{x}, \omega) = (E^1(\vec{x}, \omega), \ldots, E^d(\vec{x}, \omega))$ are mapped to vector valued functions $E^j(\vec{x}, \omega) \mapsto \vec{E}^j(\omega) = (E_1^j(\omega), \ldots, E_{L^d}^j(\omega))$ so that

$$\Theta(\vec{E}(\vec{x}, \omega)) = (\vec{E}^1(\omega), \ldots, \vec{E}^d(\omega)) \in \mathbb{C}^N, \quad N = dL^d, \tag{2.29}$$

for each $\omega \in \Omega$, and similarly for $\vec{J}(\vec{x}, \omega)$. Moreover, the bijection Θ maps the standard basis vector $\vec{e}_1 = (1, 0, \ldots, 0) \in \mathbb{Z}^d$, for example, to the vector $(\vec{1}, \vec{0}, \ldots, \vec{0}) \in \mathbb{Z}^N$, where $\vec{1}$ and $\vec{0}$ are vectors of ones and zeros of length L^d, respectively, and similarly for the $\vec{e}_j$ for $j = 2, \ldots, d$. Therefore, the vectors $\hat{e}_i$, $i = 1, \ldots, d$, satisfying

$$\hat{e}_i = \Theta(\vec{e}_i)/L^{d/2}, \qquad \hat{e}_i \cdot \hat{e}_j = \delta_{ij}, \tag{2.30}$$

serve as the standard basis vectors on $\mathbb{N}_L$.

On $\mathbb{N}_L$, the difference operators $D_j^\pm$, $j = 1, \ldots, d$, in Equation (2.24) are given in terms of finite difference matrices D_j [23], where the rows of D_j correspond to the bonds of the lattice, the columns correspond to the nodes, and the numbering of the nodes on $\mathbb{N}_L$ is determined by the bijection Θ in (2.28). In this finite lattice setting, the Laplacian Δ and the projection operator Γ in (2.26) are replaced by the real-symmetric matrices $\Delta = \nabla^T \nabla$ and $\Gamma = \nabla(\Delta^{-1})\nabla^T$, respectively, where $\nabla^T = (D_1^T, \ldots, D_d^T)$. The matrices Δ and Γ depend only on the topology and the boundary conditions of the underlying finite bond lattice and Γ is a projection matrix satisfying $\Gamma^2 = \Gamma$.

The matrix Γ is invariant under arbitrary permutations in the numbering of the nodes on $\mathbb{N}_L$, and is therefore independent of the specific form of the bijective mapping $\Theta : \mathbb{Z}_L^d \mapsto \mathbb{N}_L$ in Equation (2.28). More specifically, let Ξ be a permutation matrix

satisfying $\Xi^{-1} = \Xi^T$ such that $\vec{\xi}^T \Xi$ is the vector $\vec{\xi}^T$ with the entries permuted in an arbitrary manner. Such a permutation in the numbering of the nodes is equivalent to the mapping $D_j \mapsto D_j \Xi$, $j = 1, \ldots, d$. By the properties of transposition and inversion for products of matrices [44], it is easily verified that the matrix $\Gamma = \nabla(\Delta^{-1})\nabla^T$ is invariant under this mapping. Similarly, permuting the numbering of the bonds is equivalent to the mapping $D_j \mapsto \Xi D_j$, and under this mapping $\Gamma \mapsto \Xi \Gamma \Xi^T$.

The projection matrix representation of the operator Υ for the lattice setting is obtained as follows. For simplicity, we restrict our attention to $d = 2, 3$. For $d = 3$, the curl operation $\vec{\nabla} \times$ is given by

$$\vec{\nabla} \times \vec{\zeta} = \det \begin{bmatrix} \vec{e}_1 & \vec{e}_2 & \vec{e}_3 \\ \partial_1 & \partial_2 & \partial_3 \\ \zeta_1 & \zeta_2 & \zeta_3 \end{bmatrix} = C\vec{\zeta}, \quad C = \begin{bmatrix} 0 & -\partial_3 & \partial_2 \\ \partial_3 & 0 & -\partial_1 \\ -\partial_2 & \partial_1 & 0 \end{bmatrix}, \tag{2.31}$$

where $\vec{\zeta} = \vec{\zeta}(\vec{x})$ for $\vec{x} \in \mathbb{R}^3$, we have denoted ∂_i, $i = 1, 2, 3$, to be partial differentiation in the ith direction $\vec{e}_i$, and C is the curl operator $\vec{\nabla} \times$ in matrix form. One can check directly that $C^2 = -C^T C = -\boldsymbol{\Delta} + \vec{\nabla}\vec{\nabla}\cdot$, where $\boldsymbol{\Delta}$ is the vector Laplacian. The two-dimensional case follows from (2.31) by setting $\vec{\zeta}(\vec{x}) = [\zeta_1(\vec{x}), \zeta_2(\vec{x}), 0]^T$ with $\vec{x} = [x_1, x_2, 0]^T$, yielding

$$\vec{\nabla} \times \vec{\zeta} = (\partial_1 \zeta_2 - \partial_2 \zeta_1)\vec{e}_3 = (\vec{\nabla} \cdot R\vec{\zeta}_2)\vec{e}_3, \quad \vec{\nabla}\cdot = \begin{bmatrix} \partial_1 & \partial_2 \end{bmatrix}, \quad R = \begin{bmatrix} 0 & 1 \\ -1 & 0 \end{bmatrix}, \tag{2.32}$$

where R is a $90°$ rotation matrix, we have defined $\vec{\zeta}_2 = [\zeta_1\ \zeta_2]^T$, and the action of $\vec{\nabla} \cdot R$ on $\vec{\zeta}_2$ is given by that of the operator $[-\partial_2\ \partial_1]$.

In view of equations (2.25) and (2.31), the matrix representation of the curl operator $\vec{\nabla} \times$ for the *infinite* lattice setting on $\mathbb{Z}^3$ is given by C in (2.31) under the mapping $\partial_i \mapsto D_i^+$, $i = 1, 2, 3$, while on $\mathbb{N}_L$ the curl operator is given by C in (2.31) under the mapping $\partial_i \mapsto D_i$. In two dimensions, pointwise rotations of fields by $90°$ convert curl free fields to divergence free fields, and vice versa [56]. With this in mind and in view of Equation (2.32), in *two-dimensions* it is natural to define the curl operator by $\vec{\nabla} \times = \vec{\nabla} \cdot R = [-\partial_2\ \partial_1]$. Consequently, for the infinite lattice setting on $\mathbb{Z}^2$ we have $\vec{\nabla} \times = [-D_2^+\ D_1^+]$, while on $\mathbb{N}_L$ we have

$$\vec{\nabla} \times \vec{\zeta} = C\vec{\zeta}, \quad C^T = \begin{bmatrix} -D_2^T\ D_1^T \end{bmatrix}, \tag{2.33}$$

where $C^T C = \nabla^T \nabla = \Delta$, the matrix representation of the Laplacian. From the above discussion and in view of Equation (2.10), in the lattice setting, it is natural to define the operator Υ as

$$\Upsilon = \vec{\nabla} \times (\vec{\nabla} \times \vec{\nabla} \times)^{-1} \vec{\nabla} \times = C(C^T C)^{-1} C^T, \tag{2.34}$$

which is clearly a projection operator satisfying $\Upsilon^2 = \Upsilon$. With this definition of curl and Υ for *two dimensions*, we have $\Upsilon = R^T \Gamma R$.

Analogous to the properties of the matrix Γ, in the finite lattice setting the matrix Υ is invariant under arbitrary permutations in the numbering of the nodes. More specifically, let Ξ be defined as above and define $\boldsymbol{\Xi} = \text{diag}(\Xi, \ldots, \Xi)$, so that $\boldsymbol{\Xi}^{-1} = \boldsymbol{\Xi}^T$. Such a permutation in the numbering of the nodes is equivalent to the mapping $C \mapsto C\boldsymbol{\Xi}$. It is straight forward to verify that Υ is invariant under this mapping. Similarly, permuting the numbering of the bonds is equivalent to the mapping $C \mapsto \boldsymbol{\Xi} C$, and under this mapping $\Upsilon \mapsto \boldsymbol{\Xi} \Upsilon \boldsymbol{\Xi}^T$.

We now discuss the matrix representation of the characteristic function $\chi_1^j(\vec{x},\omega)$ on $\mathbb{N}_L$. By writing the constitutive relation $J^j(\vec{x},\omega) = \sigma^j(\vec{x},\omega)E^j(\vec{x},\omega)$ displayed in Equation (2.25) as $J^j(\vec{x},\omega) = \sigma_2(1-\chi_1^j(\vec{x},\omega)/s)E^j(\vec{x},\omega)$, we see that the characteristic function $\chi_1^j(\vec{x},\omega)$ in (2.23) operates on the electric field $E^j(\vec{x},\omega)$ in each individual bond $j = 1,\ldots,d$ emanating from $\vec{x} \in \mathbb{Z}_L^d$. In view of this and Equation (2.29), on $\mathbb{N}_L$ the characteristic function $\chi_1^j(\vec{x},\omega)$ is represented by a block diagonal matrix $\chi_1(\omega)$,

$$\chi_1(\omega) = \mathrm{diag}(\chi_1^1(\omega),\ldots,\chi_1^d(\omega)), \qquad \chi_2(\omega) = I - \chi_1(\omega), \tag{2.35}$$

where $\chi_1^j(\omega)$, $j = 1,\ldots,d$, is a *diagonal* matrix of size $L^d \times L^d$ with zeros and ones distributed according to P along the main diagonal and I is the identity matrix on $\mathbb{R}^N$. Moreover, the matrix $\chi_1^j(\omega)$ acts on the vector $\vec{E}^j(\omega) = \Theta(E^j(\vec{x},\omega))$ in (2.29) for each $j = 1,\ldots,d$. Consequently, $\chi_1(\omega)$ is also a real-symmetric projection matrix of size $N \times N$, which determines the geometry and component connectivity of the two-phase random medium. In summary, on $\mathbb{N}_L$ the operators $M_1 = \chi_1\Gamma\chi_1$ and $K_1 = \chi_1\Upsilon\chi_1$ are represented by real-symmetric random matrices of size $N \times N$ [32, 58]. The matrix representations of the operators $M_2 = \chi_2\Gamma\chi_2$ and $K_2 = \chi_2\Upsilon\chi_2$ are then determined by the relation $\chi_2(\omega) = I - \chi_1(\omega)$.

The following theorem provides a rigorous mathematical formulation of integral representations for the effective parameters of two-phase random media with finite lattice composite microstructure. The theorem and proof are formulated in terms of the random matrix $M_1 = \chi_1\Gamma\chi_1$. The formulations involving the matrices $M_2 = \chi_2\Gamma\chi_2$ and $K_i = \chi_i\Upsilon\chi_i$, $i = 1,2$, are analogous.

THEOREM 2.1. *For each $\omega \in \Omega$, let $M_1(\omega) = U(\omega)\Lambda(\omega)U(\omega)$ be the eigenvalue decomposition of the real-symmetric matrix $M_1(\omega) = \chi_1(\omega)\Gamma\chi_1(\omega)$. Here, the columns of the matrix $U(\omega)$ consist of the orthonormal eigenvectors $\vec{u}_i(\omega)$, $i = 1,\ldots,N$, of $M_1(\omega)$ and the diagonal matrix $\Lambda(\omega) = \mathrm{diag}(\lambda_1(\omega),\ldots,\lambda_N(\omega))$ involves its eigenvalues $\lambda_i(\omega)$. If the electric field $\vec{E}(\omega)$ satisfies $\vec{E}(\omega) = \vec{E}_0 + \vec{E}_f(\omega)$, with $\vec{E}_0 = \langle\vec{E}(\omega)\rangle$ and $\Gamma\vec{E}(\omega) = \vec{E}_f(\omega)$, then the effective complex conductivity tensor $\boldsymbol{\sigma}^*$ has components $\sigma_{jk}^* = \sigma_2 m_{jk}(h)$, $j,k = 1,\ldots,d$, which satisfy*

$$m_{jk}(h) = \delta_{jk} - F_{jk}(s), \quad F_{jk}(s) = \int_0^1 \frac{\mathrm{d}\mu_{jk}(\lambda)}{s-\lambda}, \quad \mathrm{d}\mu_{jk}(\lambda) = \sum_{i=1}^N \langle\delta_{\lambda_i}(\mathrm{d}\lambda)\,\chi_1\,Q_i\hat{e}_j \cdot \hat{e}_k\rangle,$$
$$\tag{2.36}$$

where $Q_i = \vec{u}_i\vec{u}_i^T$. Furthermore, the mass μ_{jk}^0 of the measure μ_{jk} satisfies

$$\mu_{jk}^0 = \langle\chi_1\hat{e}_k \cdot \hat{e}_k\rangle\delta_{jk} = d\,p_1^k\delta_{jk}. \tag{2.37}$$

Here, we have defined $p_1^k = \langle N_1^k(\omega)\rangle/N$ to be the average number fraction of type-one bonds in the positive k^{th} direction, $N_1^k(\omega) = \mathrm{Trace}(\chi_1^k(\omega))$ is the total number such bonds for $\omega \in \Omega$, and the matrix $\chi_1^k(\omega)$ is defined in Equation (2.35).

Taking $\vec{E} = \vec{E}_0 + \vec{E}_f$ with the condition $\Gamma\vec{E} = \vec{E}_f$ as a definition greatly simplifies the proof of Theorem 2.1, by avoiding the formulation and proof of some technical lemmas regarding the commutativity of the matrices D_i, D_i^T, $i = 1,\ldots,d$, and (Δ^{-1}). To assume the condition $\Gamma\vec{E} = \vec{E}_f$ is natural, as we showed in Equation (2.19) that it is a sufficient condition for the energy constraint $\langle\vec{J} \cdot \vec{E}_f\rangle = 0$, which is at the heart of the existence of solutions to the systems of equations in (2.4) and (2.25) in the infinite, continuum and

lattice settings, respectively. In the finite lattice setting, where Γ and χ_1 are matrices, this condition leads to Equation (2.11) exactly as in Section 2.1.

The proof of Theorem 2.1 is given in Section 2.2.4, after we present a novel formulation of the ACM in Section 2.2.3, which unifies the infinite settings and the finite lattice setting and makes the proof of Theorem 2.1 more transparent. Before we do so, we first introduce an important class of composite microstructures. Namely, the class of finite bond lattices such that $N_1^k(\omega)$ is a non-random constant N_1^k for all $k = 1, \ldots, d$, i.e., $N_1^k(\omega) = N_1^k$ for all $\omega \in \Omega$. Consequently, the number $N_1(\omega) = \text{Trace}(\chi_1(\omega))$ of ones along the main diagonal of $\chi_1(\omega)$ satisfies $N_1(\omega) = N_1$ for all $\omega \in \Omega$, with $N_1 = \sum_k N_1^k$. Moreover, the number fraction of type-one bonds in the kth positive direction is given by $p_1^k = N_1^k/N$ and the total number fraction of type-one bonds is given by $p_1 = N_1/N$, with $p_1 = \sum_k p_1^k$.

Given a fixed number fraction p_1 of type-one bonds, one can define a class of highly *anisotropic* composites by fixing p_1^k close to p_1 for some $k = 1, \ldots, d$, i.e., $p_1 - p_1^k \ll 1$. A class of *locally isotropic* random media is obtained by requiring that every bond emanating from $\vec{x} \in \mathbb{Z}_L^d$ in the positive direction is of the same type, i.e., $\chi_1^j(\omega) = \chi_1^k(\omega)$ for all $j, k = 1, \ldots, d$ and $\omega \in \Omega$. Hence $N_1^j = N_1^k$ for all $j, k = 1, \ldots, d$, so that $N_1^k = N_1/d$ and $p_1^k = p_1/d$ for all $k = 1, \ldots, d$. In this case, Equation (2.37) reduces to

$$\mu_{jk}^0 = p_1 \delta_{jk}, \tag{2.38}$$

which is a direct analogue of Equation (2.16). Equation (2.38) also holds for *statistically isotropic* random media, where the total number N_1 of type-one bonds is fixed and randomly distributed in a uniform fashion among the total number N of bonds. In other words, the main diagonals of the matrices $\chi_1(\omega)$, $\omega \in \Omega$, are random permutations of one another. In this case, the $N_1^k(\omega)$, $k = 1, \ldots, d$, are independent, identically distributed random variables with mean $\langle N_1^k(\omega) \rangle = p_1 N/d$.

We note that, by the law of large numbers [25], the formula $\mu_{jk}^0 = d p_1^k \delta_{jk}$ in Equation (2.37) also holds in the infinite lattice setting, where $p_1^k = \lim_{N \to \infty} \langle N_1^k(\omega) \rangle / N$ is the volume fraction of type-one bonds in the kth direction. Here, the infinite lattice is obtained as the infinite volume limit $L \to \infty$ ($N \to \infty$) of the finite lattice – with $\mathbb{Z}_L^d$ in (2.27) redefined in a suitable way so that $\lim_{L \to \infty} \mathbb{Z}_L^d = \mathbb{Z}^d$. Consequently, Equation (2.38) also holds in the infinite lattice setting for locally and statistically isotropic random media.

2.2.3. Unifying formulation of the ACM for the finite lattice setting and the infinite settings.   When considering the formulation of Stieltjes integral representations for the effective parameters of two-phase random media with finite lattice composite microstructure, there is a fundamental issue with the original formulation of the ACM given in sections 2.1 and 2.2.1. Namely, the original formulation [33] holds for the *infinite* continuum and lattice settings, but it is incompatible with the *finite* lattice setting of Section 2.2.2. In this section, we address this issue by providing a novel formulation of the ACM, which is equivalent to the original formulation and holds for both the finite lattice setting and the infinite settings.

In the infinite settings, the (infinite-dimensional) operator $\Gamma \chi_1$ appears in the bilinear functional underlying the Stieltjes integral representation for the effective conductivity tensor $\boldsymbol{\sigma}^* = \sigma_2 \mathbf{m}(h)$, displayed in Equation (2.12). The underlying Hilbert space is $\mathscr{H}_\times$, defined in (2.2), equipped with the $\mathscr{H}$-inner-product weighted by the characteristic function χ_1, and $\Gamma \chi_1$ is a self-adjoint operator on $\mathscr{H}_\times$ with respect to this inner-product. In this abstract (infinite-dimensional) Hilbert space formulation of the

effective parameter problem, the resolvent $(sI - \Gamma\chi_1)^{-1}$ is also self-adjoint with respect to this inner-product for $s \in \mathbb{C} \backslash [0,1]$ [72].

In contrast, the finite lattice formulation of the effective parameter problem involves a finite dimensional Hilbert space and the operators Γ and χ_1 are real-symmetric, non-commutable matrices. In this case, the matrix $\Gamma\chi_1$ is *not* symmetric, it typically has complex spectrum, and it may not even have a full set of eigenvectors. Consequently, the resolvent $(sI - \Gamma\chi_1)^{-1}$ of this matrix is not symmetric and, in general, is not defined for all $s \in \mathbb{C} \backslash [0,1]$ as required. Therefore, the integral formula of Theorem 2.1 displayed in Equation (2.36), which follows from the spectral theorem displayed in Equation (A.4) for the *real-symmetric* matrix $\chi_1\Gamma\chi_1$, fails to hold for the matrix $\Gamma\chi_1$, in general. Due to this fundamental difference of the finite lattice setting, the mathematical framework must be modified from that of the infinite settings discussed in sections 2.1 and 2.2.1.

We now develop a novel formulation of the ACM which holds for both the finite lattice setting and the infinite settings, and yields the integral representations for the effective parameters displayed in equations (2.12) and (2.36). To make the formulation independent of the setting, whether finite or infinite, we make use of generic terms such as symmetric operator, for example, which means real-symmetric matrix in the finite lattice setting and self-adjoint operator in the infinite settings. Essential differences in notation will be explicitly stated.

Recall the definition of the effective conductivity tensor $\langle \vec{J} \rangle = \langle \sigma \vec{E} \rangle = \boldsymbol{\sigma}^* \langle \vec{E} \rangle$ and that $\sigma = \sigma_2(1 - \chi_1/s)$ and $\langle \vec{E} \rangle = \vec{E}_0$, together yielding

$$\boldsymbol{\sigma}^* \vec{E}_0 = \sigma_2(\vec{E}_0 - \langle \chi_1 \vec{E} \rangle / s). \tag{2.39}$$

Define the coordinate system so that $\vec{E}_0 = E_0 \vec{e}_j$ for some $j = 1, \ldots, d$ (in the matrix formulation $\vec{e}_j \mapsto \hat{e}_j$, where $\hat{e}_j$ is defined in Equation (2.30)). Therefore, taking the dot product of equation (2.39) with the (non-random) basis vector $\vec{e}_k$ yields

$$\sigma_{jk}^* = \boldsymbol{\sigma}^* \vec{e}_j \cdot \vec{e}_k = \sigma_2 \left(\delta_{jk} - \langle \chi_1 \vec{E} \cdot \vec{e}_k \rangle / (sE_0) \right). \tag{2.40}$$

This demonstrates that the key functional underlying the Stieltjes integral representation for the effective complex conductivity tensor is $\langle \chi_1 \vec{E} \cdot \vec{e}_k \rangle$. In fact, in view of equations (2.12) and (2.40), we have that $F_{jk}(s) = \langle \chi_1 \vec{E} \cdot \vec{e}_k \rangle / (sE_0)$.

We now derive a resolvent formula for the vector field $\chi_1 \vec{E}$ involving the symmetric operator $\chi_1 \Gamma \chi_1$. With use of the identity $\vec{E} = \vec{E}_0 + \vec{E}_f$ we rewrite the first formula of Equation (2.11) as

$$(sI - \Gamma\chi_1)\vec{E} = s\vec{E}_0, \tag{2.41}$$

where I is the identity operator on the underlying vector space ($\mathbb{R}^d$ for the infinite settings and $\mathbb{R}^N$ for the finite lattice setting). It is now clear that the formula for $m_{jk}(h) = \sigma_{jk}^*/\sigma_2$ displayed in (2.12) follows by writing the formula in Equation (2.41) as $\vec{E} = s(sI - \Gamma\chi_1)^{-1}\vec{E}_0$ with $\vec{E}_0 = E_0\vec{e}_j$, and substituting this into (2.40). We wish to derive an analogous formula for $m_{jk}(h)$ involving the symmetric operator $\chi_1 \Gamma \chi_1$. In order to introduce this operator and to isolate $\chi_1 \vec{E}$ in Equation (2.41), we premultiply this formula by the *projection* operator χ_1, yielding

$$(sI - \chi_1\Gamma\chi_1)[\chi_1\vec{E}] = s\chi_1\vec{E}_0. \tag{2.42}$$

Equation (2.42) is equivalent to the following resolvent formula for $\chi_1 \vec{E}$:

$$\chi_1 \vec{E} = s(sI - \chi_1 \Gamma \chi_1)^{-1} \chi_1 \vec{E}_0, \tag{2.43}$$

which is analogous to that of Equation (2.9) for the electric field $\vec{E}$. Inserting the resolvent formula for $\chi_1 \vec{E}$ in (2.43), with $\vec{E}_0 = E_0 \vec{e}_j$, into Equation (2.40) yields $F_{jk}(s) = \langle (sI - \chi_1 \Gamma \chi_1)^{-1} \chi_1 \vec{e}_j \cdot \vec{e}_k \rangle$, which is a bilinear functional representation of the function $F_{jk}(s)$. Now, applying the spectral theorem for the symmetric operator $\chi_1 \Gamma \chi_1$, displayed in equations (A.2) and (A.4) with $f(\lambda) = (s - \lambda)^{-1}$ and $g(\lambda) \equiv 1$, to this functional representation of $F_{jk}(s)$ yields the following Stieltjes integral representation for $m_{jk}(h) = \sigma_{jk}^*/\sigma_2$:

$$m_{jk}(h) = \delta_{jk} - F_{jk}(s), \qquad F_{jk}(s) = \langle (sI - \chi_1 \Gamma \chi_1)^{-1} \chi_1 \vec{e}_j \cdot \vec{e}_k \rangle = \int_0^1 \frac{\mathrm{d}\mu_{jk}(\lambda)}{s - \lambda}. \tag{2.44}$$

Equation (2.44) demonstrates, as in Section 2.1, that the Hilbert space underlying the integral representation for σ_{jk}^* is given by $\mathscr{H}_\times$ equipped with the $\mathscr{H}$-inner-product weighted by χ_1. However, in Section 2.1, the weighting of the inner-product is defined by premultiplication of χ_1, so that $\langle f(\Gamma \chi_1) \vec{e}_j, \vec{e}_k \rangle_1 = \langle \chi_1 f(\Gamma \chi_1) \vec{e}_j \cdot \vec{e}_k \rangle$ for all complex valued functions $f \in L^2(\mu_{jk})$ [72]. Here, the weighting of the inner-product is defined by post multiplication of χ_1, so that the inner-product $\langle \cdot, \cdot \rangle_1$ is instead given by $\langle f(\chi_1 \Gamma \chi_1) \vec{e}_j, \vec{e}_k \rangle_1 = \langle f(\chi_1 \Gamma \chi_1) \chi_1 \vec{e}_j \cdot \vec{e}_k \rangle$. In the infinite, continuum and lattice settings, the two inner-product definitions are equivalent, as χ_1 acts *pointwise* on the underlying vector space ($\mathbb{R}^d$ in the continuous setting and $\mathbb{Z}^d$ in the lattice setting). However, in the finite lattice setting where χ_1 is represented by a matrix, the two inner-product definitions are no longer equivalent for all such functions f.

We now establish that the formula for $m_{jk}(h)$ displayed in Equation (2.44) is equivalent to that of Equation (2.12) for the infinite, continuum and lattice settings. From Equation (2.12) write $F_{jk}(s; \mu_{jk}) = \langle \chi_1 (sI - \Gamma \chi_1)^{-1} \vec{e}_j \cdot \vec{e}_k \rangle$ and from Equation (2.44) write $\tilde{F}_{jk}(s; \nu_{jk}) = \langle (sI - \chi_1 \Gamma \chi_1)^{-1} \chi_1 \vec{e}_j \cdot \vec{e}_k \rangle$. We will argue that $\mu_{jk} \equiv \nu_{jk}$ so that $F_{jk}(s; \mu_{jk}) \equiv \tilde{F}_{jk}(s; \nu_{jk})$. From the spectral theorem, we have that the moments μ_{jk}^n and ν_{jk}^n, $n = 0, 1, 2, \ldots$, of the measures μ_{jk} and ν_{jk} satisfy

$$\mu_{jk}^n = \int_0^1 \lambda^n \mathrm{d}\mu_{jk}(\lambda) = \langle \chi_1 [\Gamma \chi_1]^n \vec{e}_j \cdot \vec{e}_k \rangle, \qquad \nu_{jk}^n = \int_0^1 \lambda^n \mathrm{d}\nu_{jk}(\lambda) = \langle [\chi_1 \Gamma \chi_1]^n \chi_1 \vec{e}_j \cdot \vec{e}_k \rangle. \tag{2.45}$$

However, since χ_1 is a projection operator, we have that $\chi_1 = \chi_1^m$ on $\mathscr{H}_\times$ for all $m \in \mathbb{N}$, hence $\chi_1 [\Gamma \chi_1]^n = [\chi_1 \Gamma \chi_1]^n \chi_1$ on $\mathscr{H}_\times$ for all $n = 0, 1, 2, \ldots$. This and Equation (2.45) imply that $\mu_{jk}^n \equiv \nu_{jk}^n$ for all $n = 0, 1, 2, \ldots$. Since the Hausdorff moment problem is determined [67], i.e., knowledge of all the moments uniquely determines the measure, we have that $\mu_{jk} \equiv \nu_{jk}$. This, in turn, implies that $F_{jk}(s; \mu_{jk}) \equiv \tilde{F}_{jk}(s; \nu_{jk})$, which is what we set out to establish.

2.2.4. Proof of Theorem 2.1.

Proof. In this section, we prove the various assertions of Theorem 2.1, which was stated in Section 2.2.2. In particular, we prove that the functional $F_{jk}(s) = \langle (sI - \chi_1 \Gamma \chi_1)^{-1} \chi_1 \hat{e}_j \cdot \hat{e}_k \rangle$ in (2.44) (with $\vec{e}_j \mapsto \hat{e}_j$) has the integral representation displayed in Equation (2.36), involving a spectral measure μ_{jk} of the real-symmetric matrix $\chi_1 \Gamma \chi_1$ with mass μ_{jk}^0 given by that in (2.37). We also provide a projection method

for numerically efficient, rigorous computation of μ_{jk}. This projection method is summarized by equations (2.57)–(2.59) below.

Toward this goal, for each $\omega \in \Omega$ define the sets $\mathbb{N}_L^1(\omega)$ and $\mathbb{N}_L^0(\omega)$ by

$$\mathbb{N}_L^1(\omega) = \{i \in \mathbb{N}_L \mid [\chi_1(\omega)]_{ii} = 1\}, \qquad \mathbb{N}_L^0(\omega) = \mathbb{N}_L \backslash \mathbb{N}_L^1(\omega). \qquad (2.46)$$

Also, define elementary permutation matrices [23] $\Pi_{\ell m}(\omega)$, $\ell, m = 1, \ldots, N$, $N = dL^d$, which satisfy $\Pi_{\ell m} = \Pi_{\ell m}^{-1} = \Pi_{\ell m}^T$ and $\Pi_{\ell m}\vec{\xi}$ is the vector $\vec{\xi}$ with the ℓth and m^{th} entries interchanged. Since $\chi_1(\omega)$ is a diagonal matrix with $N_1(\omega)$ ones and $N_0(\omega) = N - N_1(\omega)$ zeros along its main diagonal, it is clear that there exists a permutation matrix $\Pi(\omega)$ which is a composition of elementary permutation matrices such that

$$\Pi\chi_1\Pi^T = \begin{bmatrix} 0_{00} & 0_{01} \\ 0_{10} & I_1 \end{bmatrix}, \qquad \Pi = \prod_{\ell, m \in \mathbb{N}_L} \Pi_{\ell m}, \qquad (2.47)$$

where $\ell \in \mathbb{N}_L^1$, $m \in \mathbb{N}_L^0$, I_1 is the identity matrix of size $N_1 \times N_1$, and 0_{ab} is a matrix of zeros of size $N_a \times N_b$, for $a, b = 0, 1$. Therefore, since $\Pi^T = \Pi^{-1}$ we have

$$\chi_1\Gamma\chi_1 = \Pi^T \begin{bmatrix} 0_{00} & 0_{01} \\ 0_{10} & I_1 \end{bmatrix} \Gamma_\Pi \begin{bmatrix} 0_{00} & 0_{01} \\ 0_{10} & I_1 \end{bmatrix} \Pi = \Pi^T \begin{bmatrix} 0_{00} & 0_{01} \\ 0_{10} & \Gamma_1 \end{bmatrix} \Pi = \Pi^T \begin{bmatrix} 0_{00} & 0_{01} \\ 0_{10} & U_1\Lambda_1 U_1^T \end{bmatrix} \Pi$$

$$= \Pi^T \begin{bmatrix} I_0 & 0_{01} \\ 0_{10} & U_1 \end{bmatrix} \begin{bmatrix} 0_{00} & 0_{01} \\ 0_{10} & \Lambda_1 \end{bmatrix} \begin{bmatrix} I_0 & 0_{01} \\ 0_{10} & U_1^T \end{bmatrix} \Pi, \qquad (2.48)$$

where I_0 is the identity matrix of size $N_0 \times N_0$. Here, we have defined the real-symmetric matrix $\Gamma_\Pi = \Pi\Gamma\Pi^T$, Γ_1 is its lower right principal sub-matrix of size $N_1 \times N_1$, and $\Gamma_1 = U_1\Lambda_1 U_1^T$ is the eigenvalue decomposition of Γ_1. As Γ_1 is a real-symmetric matrix, U_1 is an orthogonal matrix [44]. Also, since $\Gamma_\Pi = \Pi\Gamma\Pi^T$ is a similarity transformation of a projection matrix and $\Pi\chi_1\Pi^T$ is a projection matrix, Λ_1 is a diagonal matrix with entries $\lambda_i^1 \in [0, 1]$, $i = 1, \ldots, N_1$, along its diagonal [44, 23].

Consequently, Equation (2.48) implies that the eigenvalue decomposition of the matrix $\chi_1\Gamma\chi_1$ is given by

$$\chi_1\Gamma\chi_1 = U\Lambda U^T, \qquad U = \Pi^T \begin{bmatrix} I_0 & 0_{01} \\ 0_{10} & U_1 \end{bmatrix}, \qquad \Lambda = \begin{bmatrix} 0_{00} & 0_{01} \\ 0_{10} & \Lambda_1 \end{bmatrix}. \qquad (2.49)$$

Here, U is an orthogonal matrix satisfying $U^T U = UU^T = I$, I is the identity matrix on $\mathbb{R}^N$, and Λ is a diagonal matrix with entries $\lambda_i \in [0, 1]$, $i = 1, \ldots, N$, along its diagonal.

The eigenvalue decomposition of the matrix $\chi_1\Gamma\chi_1$ displayed in Equation (2.49) demonstrates that its resolvent $(sI - \chi_1\Gamma\chi_1)^{-1}$ is well defined for all $s \in \mathbb{C}\backslash[0, 1]$. In particular, by the orthogonality of the matrix U, it has the following useful representation $(sI - \chi_1\Gamma\chi_1)^{-1} = U(sI - \Lambda)^{-1}U^T$, where $(sI - \Lambda)^{-1}$ is a diagonal matrix with entries $1/(s - \lambda_i)$ along its diagonal. This, in turn, implies that the functional $F_{jk}(s) = \langle (sI - \chi_1\Gamma\chi_1)^{-1}\chi_1\hat{e}_j \cdot \hat{e}_k \rangle$ displayed in Equation (2.44) (with $\vec{e}_j \mapsto \hat{e}_j$) can be written as

$$F_{jk}(s) = \langle (sI - \Lambda)^{-1}[\chi_1 U]^T \hat{e}_j \cdot U^T \hat{e}_k \rangle. \qquad (2.50)$$

Since $\Pi^T = \Pi^{-1}$, equations (2.47) and (2.49) imply that

$$\chi_1 U = \Pi^T \begin{bmatrix} 0_{00} & 0_{01} \\ 0_{10} & U_1 \end{bmatrix} \implies \chi_1\vec{u}_i = \begin{cases} 0, & \text{for } i = 1, \ldots, N_0, \\ \vec{u}_i, & \text{otherwise.} \end{cases} \qquad (2.51)$$

This, in turn, implies that

$$[\chi_1 U]^T \hat{e}_j \cdot U^T \hat{e}_k = [\chi_1 U]^T \hat{e}_j \cdot [\chi_1 U]^T \hat{e}_k. \tag{2.52}$$

We are ready to provide the integral representation displayed in (2.36) for the functional $F_{jk}(s)$ in Equation (2.50). Denote by $Q_i = \vec{u}_i \vec{u}_i^T$, $i = 1, \ldots, N$, the symmetric, mutually orthogonal projection matrices, $Q_\ell Q_m = Q_\ell \delta_{\ell m}$, onto the eigen-spaces spanned by the orthonormal eigenvectors $\vec{u}_i$. Equation (2.51) implies that $\chi_1 Q_i = Q_i \chi_1 = \chi_1 Q_i \chi_1$, as $\chi_1 Q_i = 0$ for $i = 1, \ldots, N_0$ and $\chi_1 Q_i = Q_i$ otherwise. This allows us to write the quadratic form $[\chi_1 U]^T \hat{e}_j \cdot [\chi_1 U]^T \hat{e}_k$ as

$$[\chi_1 U]^T \hat{e}_j \cdot [\chi_1 U]^T \hat{e}_k = \sum_{i=1}^N (\chi_1 \vec{u}_i \cdot \hat{e}_j)(\chi_1 \vec{u}_i \cdot \hat{e}_k) = \sum_{i=1}^N \chi_1 Q_i \chi_1 \hat{e}_j \cdot \hat{e}_k = \sum_{i=1}^N \chi_1 Q_i \hat{e}_j \cdot \hat{e}_k. \tag{2.53}$$

This and equations (2.50) and (2.52) yield

$$F_{jk}(s) = \int_0^1 \frac{\mathrm{d}\mu_{jk}(\lambda)}{s - \lambda}, \quad \mathrm{d}\mu_{jk}(\lambda) = \sum_{i=1}^N \langle \delta_{\lambda_i}(\mathrm{d}\lambda)\, \chi_1 Q_i \hat{e}_j \cdot \hat{e}_k \rangle. \tag{2.54}$$

From Equation (A.3) we have that $\sum_i Q_i = I$, which implies that the mass μ_{jk}^0 of the measure μ_{jk} is given by

$$\mu_{jk}^0 = \int_0^1 \mathrm{d}\mu_{jk}(\lambda) = \int_0^1 \sum_{i=1}^N \langle \delta_{\lambda_i}(\mathrm{d}\lambda)\chi_1 Q_i \hat{e}_j \cdot \hat{e}_k \rangle = \langle \chi_1 \hat{e}_j \cdot \hat{e}_k \rangle = \langle \chi_1 \hat{e}_k \cdot \hat{e}_k \rangle \delta_{jk}, \tag{2.55}$$

as χ_1 is a diagonal matrix and the underlying probability space is finite. Therefore, as in the continuum setting, the diagonal components μ_{kk} of the matrix valued measure $\boldsymbol{\mu}$ are positive measures with mass $\langle \chi_1 \hat{e}_k \cdot \hat{e}_k \rangle = \langle \chi_1 \hat{e}_k \cdot \chi_1 \hat{e}_k \rangle = \langle |\chi_1 \hat{e}_k|^2 \rangle \geq 0$, as χ_1 is a symmetric projection matrix. The off-diagonal components μ_{jk}, for $j \neq k$, have zero mass and are consequently signed measures.

Using Equation (2.35), we may write μ_{jk}^0 in Equation (2.55) in a more suggestive form. Recall that $\hat{e}_1 = (\vec{1}, \vec{0}, \ldots, \vec{0})/L^{d/2}$, where $\vec{1}$ and $\vec{0}$ are vectors of ones and zeros of length L^d, respectively, and similarly for the $\vec{e}_j$ for $j = 2, \ldots, d$. Since χ_1 is a symmetric projection matrix, equations (2.35) and (2.55) imply that

$$\mu_{jk}^0 = \langle \chi_1 \hat{e}_k \cdot \chi_1 \hat{e}_k \rangle \delta_{jk} = \frac{1}{L^d} \langle \chi_1^k \vec{1} \cdot \chi_1^k \vec{1} \rangle \delta_{jk} = \frac{1}{L^d} \langle \mathrm{Trace}(\chi_1^k) \rangle \delta_{jk} = d \frac{\langle N_1^k(\omega) \rangle}{N} \delta_{jk}, \tag{2.56}$$

where $N_1^k(\omega) = \mathrm{Trace}(\chi_1^k(\omega))$ is the total number of type-one bonds in the positive k^{th} direction for $\omega \in \Omega$ and $N = dL^d$. This proves Equation (2.37) and concludes our proof of Theorem 2.1. $\qquad \square$

We conclude this section with the formulation of a projection method for numerically efficient, rigorous computation of spectral measures and effective parameters for composite media with finite lattice microstructure. Note that the sum in Equation (2.54) runs only over the index set $i = N_0 + 1, \ldots, N$, as Equation (2.51) implies that the masses $\chi_1 Q_i \hat{e}_j \cdot \hat{e}_k$ of the measure μ_{jk} are zero for $i = 1, \ldots, N_0$. Denote by λ_i^1 and $\vec{u}_i^1$, $i = 1, \ldots, N_1$, the eigenvalues and eigenvectors of the $N_1 \times N_1$ matrix $\Gamma_1 = U_1 \Lambda_1 U_1^T$, defined in Equation (2.48). Now, write

$$\Pi \hat{e}_j = \begin{bmatrix} \hat{e}_j^{\pi_0} \\ \hat{e}_j^{\pi_1} \end{bmatrix}, \tag{2.57}$$

where $\hat{e}_j^{\pi_0} \in \mathbb{R}^{N_0}$ and $\hat{e}_j^{\pi_1} \in \mathbb{R}^{N_1}$. Therefore, writing the matrix $\chi_1 U$ in Equation (2.51) in block diagonal form, $\chi_1 U = \Pi^T \text{diag}(0_{00}, U_1)$, we have that

$$[\chi_1 U]^T \hat{e}_j \cdot [\chi_1 U]^T \hat{e}_k = [\text{diag}(0_{00}, U_1^T)\Pi\hat{e}_j] \cdot [\text{diag}(0_{0,0}, U_1^T)\Pi\hat{e}_k] = [U_1^T \hat{e}_j^{\pi_1}] \cdot [U_1^T \hat{e}_k^{\pi_1}]. \tag{2.58}$$

Denote by $Q_i^1 = \vec{u}_i^1 [\vec{u}_i^1]^T$, $i = 1, \ldots, N_1$, the mutually orthogonal projection matrices, $Q_\ell^1 Q_m^1 = Q_\ell^1 \delta_{\ell m}$, onto the eigen-spaces spanned by the orthonormal eigenvectors $\vec{u}_i^1$. Equations (2.50), (2.52), and (2.58) then yield

$$F_{jk}(s) = \langle (sI_1 - \Lambda_1)^{-1} [U_1^T \hat{e}_j^{\pi_1}] \cdot [U_1^T \hat{e}_k^{\pi_1}] \rangle = \left\langle \sum_{i=1}^{N_1} \frac{Q_i^1 \hat{e}_j^{\pi_1} \cdot \hat{e}_k^{\pi_1}}{s - \lambda_i^1} \right\rangle. \tag{2.59}$$

Equation (2.59) demonstrates that only the spectral information of the matrices U_1 and Λ_1 appear in the functional representation for $F_{jk}(s)$ in (2.50) and its integral representation in (2.36). From a computational standpoint, this means that only the eigenvalues and eigenvectors of the $N_1 \times N_1$ matrix Γ_1 need to be computed in order to compute the spectral measures underlying the integral representations of the effective parameters for finite lattice systems. This is extremely cost effective for large dilute systems, where $N \gg 1$ and $N_1 \ll N$, as the numerical cost of finding all the eigenvalues and eigenvectors of a real-symmetric $N \times N$ matrix is $O(N^3)$ [23].

2.3. Bounding procedure. In this section, we review a procedure which yields rigorous bounds for the effective transport coefficients of composite media [33, 28]. The bounding procedure associated with the functions $F_{kk}(s)$ and $E_{kk}(s)$, defined in Equation (2.12), for example, fixes the contrast parameter s and varies over admissible sets of measures μ_{kk} and η_{kk}, subject to known information regarding the composite. This information is given in terms of the moments μ_{kk}^n and η_{kk}^n, $n = 0, 1, 2, \ldots$, of these measures. Knowledge of the moments for $n = 1, \ldots, J$ confines the value of the effective complex conductivity σ_{kk}^* to a region of the complex plane which is bounded by arcs of circles, and the region becomes progressively smaller as more moments are known [55, 28]. Since the bounding procedure associated with the functions $G_{kk}(t)$ and $H_{kk}(t)$ in (2.12) is analogous, we will focus on that involving $F_{kk}(s)$ and $E_{kk}(s)$.

The bounds for σ_{kk}^* and ρ_{kk}^* follow from three important properties of the functions $F_{kk}(s)$ and $E_{kk}(s)$. First, their integral representations displayed in equations (2.12) and (2.36) *separate* parameter information in s and E_0 from the geometry of the composite, which is encoded in the underlying spectral measures μ_{kk} and η_{kk} via their moments μ_{kk}^n and η_{kk}^n, $n = 0, 1, 2, \ldots$ [11, 33]. Second, these integral representations are *linear* functionals of the spectral measures. Finally, μ_{kk} and η_{kk} are *positive* measures, in contrast to μ_{jk} and η_{jk} for $j \neq k$. In this section, we review how these three properties yield rigorous bounds for the diagonal components of the effective parameters σ_{kk}^* and ρ_{kk}^* [33, 28].

We start our discussion with the masses μ_{kk}^0 and η_{kk}^0 of the measures μ_{kk} and η_{kk} for the continuum and lattice settings. By Equation (2.16) and the symmetries between the functions $F_{kk}(s)$ and $E_{kk}(s)$ displayed in Equation (2.12), in the continuum setting, the masses μ_{kk}^0 and η_{kk}^0 of the measures μ_{kk} and η_{kk} are generically given by $\mu_{kk}^0 = p_1$ and $\eta_{kk}^0 = p_2$, so that

$$\mu_{kk}^0 + \eta_{kk}^0 = 1, \quad k = 1, \ldots, d. \tag{2.60}$$

By Equation (2.37), in the finite lattice setting, we have $\mu_{kk}^0 = dp_1^k$ generically. The masses μ_{kk}^0 and η_{kk}^0 of the measures μ_{kk} and η_{kk} are related in this finite lattice setting

as follows. From Equation (2.35) we have that $\chi_1^k(\omega) + \chi_2^k(\omega) = I_{L^d}$ for all $k = 1, \ldots, d$ and $\omega \in \Omega$, where I_{L^d} is the identity matrix of size $L^d \times L^d$. Consequently, by the linearity of the trace operation, we have that $\mathrm{Trace}(\chi_1^k(\omega)) + \mathrm{Trace}(\chi_2^k(\omega)) = \mathrm{Trace}(I_{L^d})$, thus $N_1^k(\omega) + N_2^k(\omega) = L^d = N/d$. Averaging this formula over Ω and rearranging yields Equation (2.60), where $\eta_{kk}^0 = dp_2^k$ and $p_2^k = \langle N_2^k(\omega)\rangle/N$ is the average number fraction of type-two bonds in the positive k^{th} direction. For isotropic random media with finite lattice composite microstructure, we have from (2.38) that $\mu_{kk}^0 = p_1$ and $\eta_{kk}^0 = p_2$. By the discussion in the paragraph following Equation (2.38), the formulas $\mu_{kk}^0 = dp_1^k$ and $\eta_{kk}^0 = dp_2^k$ also hold for the infinite lattice setting with $p_i^k = \lim_{N \to \infty} \langle N_i(\omega)\rangle/N$, $i = 1, 2$, and are given by $\mu_{kk}^0 = p_1$ and $\eta_{kk}^0 = p_2$ for isotropic random media.

For simplicity, we will focus on one diagonal component σ_{kk}^* and ρ_{kk}^* of the effective conductivity and resistivity tensors $\boldsymbol{\sigma}^*$ and $\boldsymbol{\rho}^*$, for some $k = 1, \ldots, d$, and set $\sigma^* = \sigma_{kk}^*$, $F(s) = F_{kk}(s)$, $m(h) = m_{kk}(h)$, $\mu = \mu_{kk}$, $E(s) = E_{kk}(s)$, $\tilde{m}(h) = \tilde{m}_{kk}(h)$, and $\eta = \eta_{kk}$. Here, $F(s) = 1 - m(h)$ and $E(s) = 1 - \tilde{m}(h)$. We will also exploit the symmetries between $F(s)$ and $E(s)$ in Equation (2.12) and initially focus on the function $F(s)$ and the measure μ, referring to the function $E(s)$ and the measure η where appropriate.

Bounds for σ^* are obtained as follows, while those for ρ^* are obtained analogously. The support of the measure μ is contained in the interval $[0,1]$ and its mass is given by $\mu^0 = p_1$, where $0 \le p_1 \le 1$. Consider the set $\mathscr{M}$ of positive Borel measures on $[0,1]$ with mass ≤ 1. By Equation (2.12), for fixed $s \in \mathbb{C} \setminus [0,1]$, $F(s)$ is a linear functional of the measure μ, $F : \mathscr{M} \mapsto \mathbb{C}$, and we write $F(s) = F(s; \mu)$ and $m(h) = m(h; \mu)$. Suppose that we know the moments μ^n of the measure μ for $n = 0, \ldots, J$. Define the set $\mathscr{M}_J^\mu \subset \mathscr{M}$ of measures by

$$\mathscr{M}_J^\mu = \left\{ \nu \in \mathscr{M} \;\Big|\; \int_0^1 \lambda^n \mathrm{d}\nu(\lambda) = \mu^n, \; n = 0, \ldots, J \right\}. \tag{2.61}$$

The set $A_J^\mu \subset \mathbb{C}$ that represents the possible values of $m(h; \mu) = 1 - F(s; \mu)$ which is compatible with the known information about the random medium is given by

$$A_J^\mu = \{\, m(h; \nu) \in \mathbb{C} \mid h \notin (-\infty, 0], \; \nu \in \mathscr{M}_J^\mu \}. \tag{2.62}$$

The set of measures $\mathscr{M}_J^\mu$ is a compact, convex subset of $\mathscr{M}$ with the topology of weak convergence [33]. Since the mapping $F(s; \mu)$ in (2.12) is linear in μ, it follows that A_J^μ is a compact convex subset of the complex plane $\mathbb{C}$. The extreme points of $\mathscr{M}_0^\mu$ are the one point measures $a\delta_b$, $0 \le a, b \le 1$ [24], while the extreme points of $\mathscr{M}_J^\mu$ for $J > 0$ are weak limits of convex combinations of measures of the form [47, 33]

$$\mu_J(\mathrm{d}\lambda) = \sum_{i=1}^{J+1} a_i \delta_{b_i}(\mathrm{d}\lambda), \quad a_i \ge 0, \quad 0 \le b_1 < \cdots < b_{J+1} < 1, \quad \sum_{i=1}^{J+1} a_i b_i^n = \mu^n, \tag{2.63}$$

for $n = 0, 1, \ldots, J$.

For the case of two-dimensional random media in the continuous setting, every measure $\mu \in \mathscr{M}_J^\mu$ gives rise to a function $m(h; \mu)$ that is the effective (relative) conductivity of a multi-rank laminate [56]. However, in general [33], not every measure $\mu \in \mathscr{M}_J^\mu$ gives rise to such a function $m(h; \mu)$. Therefore, the set A_J^μ will *contain* the exact range of values of the effective conductivity [33]. This is sufficient for the bounding procedure discussed in this section.

By the symmetries between the formulas in Equation (2.12), the support of the measure η is contained in the interval $[0,1]$ and its mass is given by $\eta^0 = p_2 = 1 - p_1$, where

$0 \le p_2 \le 1$. We can therefore define compact, convex sets $\mathcal{M}_J^\eta \subset \mathcal{M}$ and $A_J^\eta \subset \mathbb{C}$ which are analogous to those defined in equations (2.61) and (2.62), respectively, involving the function $\tilde{m}(h;\eta) = 1 - E(s;\eta)$. Moreover, the extreme points of $\mathcal{M}_0^\eta$ are the one point measures $c\delta_d$, $0 \le c,d \le 1$, while the extreme points of $\mathcal{M}_J^\eta$ are weak limits of convex combinations of measures of the form given in Equation (2.63).

Consequently, in order to determine the extreme points of the sets A_J^μ and A_J^η, it suffices to determine the range of values in $\mathbb{C}$ of the functions $m(h;\mu_J) = 1 - F(s;\mu_J)$ and $\tilde{m}(h;\eta_J) = 1 - E(s;\eta_J)$, respectively, where

$$F(s;\mu_J) = \sum_{i=1}^{J+1} \frac{a_i}{s - b_i}, \qquad E(s;\eta_J) = \sum_{i=1}^{J+1} \frac{c_i}{s - d_i}, \qquad (2.64)$$

as the a_i, b_i, c_i, and d_i vary under the constraints given in Equation (2.63). While $F(s;\mu_J)$ and $E(s;\eta_J)$ in (2.64) may not run over all points in A_J^μ and A_J^η as these parameters vary, they run over the extreme points of these sets, which is sufficient due to their convexity. It is important to note that, as the effective complex conductivity σ^* is given by $\sigma^* = \sigma_2 m(h;\mu) = \sigma_1/\tilde{m}(h;\eta)$, the regions A_J^μ and A_J^η have to be mapped to the common σ^*-plane to provide bounds for σ^*.

We will discuss the bounds for σ^* in detail for the cases where $J = 0, 1$, and briefly explain how the procedure is generalized to obtain a sequence of nested bounds for $J = 2, 3, \dots$ [28]. The bounds corresponding to the case where $J = 0$ follows from the knowledge of only the masses μ^0 and η^0 of the measures μ and η. For simplicity, we assume that $\mu^0 = p_1$ and $\eta^0 = p_2$. If the random medium is also known to be statistically isotropic, so that the effective tensors $\boldsymbol{\sigma}^*$ and $\boldsymbol{\rho}^*$ are diagonal [56], the first moments μ^1 and η^1 are also known to be given by [28]

$$\mu^1 = \frac{p_1 p_2}{d}, \qquad \eta^1 = \frac{p_1 p_2 (d-1)}{d}, \qquad (2.65)$$

which leads to bounds for the case where $J = 1$.

Consider the case where $J = 0$ in (2.64) and the volume fraction $p_1 = 1 - p_2$ is fixed with $\mu^0 = p_1$ and $\eta^0 = p_2$, so that $F(s;\mu_J) = p_1/(s-\lambda)$ and $E(s;\eta_J) = p_2/(s-\tilde{\lambda})$. By the above discussion, the values of $F(s;\mu)$ and $E(s;\eta)$ lie inside the circles $C_0(\lambda)$ and $\tilde{C}_0(\tilde{\lambda})$, respectively, given by

$$C_0(\lambda) = \frac{\mu^0}{s - \lambda}, \quad -\infty \le \lambda \le \infty, \qquad \tilde{C}_0(\tilde{\lambda}) = \frac{\eta^0}{s - \tilde{\lambda}}, \quad -\infty \le \tilde{\lambda} \le \infty. \qquad (2.66)$$

In the σ^*-plane, the intersection of these two regions is bounded by two circular arcs corresponding to $0 \le \lambda \le p_2$ and $0 \le \tilde{\lambda} \le p_1$ in (2.66), and the values of σ^* lie inside this region [28]. These bounds are optimal [54, 8], and are obtained by a composite of uniformly aligned spheroids of material 1 in all sizes coated with confocal shells of material 2, and vice versa. The arcs are traced out as the aspect ratio varies. When the value of the component conductivities σ_1 and σ_2 are real and positive, the bounding region collapses to the interval $1/(p_1/\sigma_1 + p_2/\sigma_2) \le \sigma^* \le p_1\sigma_1 + p_2\sigma_2$, which are the Wiener bounds. The lower and upper bounds are obtained by parallel slabs of the two materials aligned perpendicular and parallel to the field $\vec{E}_0$, respectively [65].

Now consider the case where $J = 1$ in (2.64). Here, the volume fraction $p_1 = 1 - p_2$ is fixed so that $\mu^0 = p_1$ and $\eta^0 = p_2$, and the random medium is statistically isotropic so that the first moments μ^1 and η^1 are given by that in Equation (2.65). A convenient

way of including this information is to use the transformations [8]

$$F_1(s) = \frac{1}{p_1} - \frac{1}{sF(s)}, \qquad E_1(s) = \frac{1}{p_2} - \frac{1}{sE(s)}. \qquad (2.67)$$

Due to the symmetries between $F_1(s)$ and $E_1(s)$ in (2.67), we will first focus on the function $F_1(s)$ and introduce the function $E_1(s)$ when appropriate. The function $F_1(s)$ is an upper half plane function analytic off $[0,1]$ and therefore has an integral representation [8, 28] analogous to that in Equation (2.12), involving a measure μ_1, say, which is supported in the interval $[0,1]$. Since only the mass $\mu^0 = p_1$ and the first moment $\mu^1 = p_1 p_2/d$ of the measure μ are known, the transformation (2.67) determines only the mass $\mu_1^0 = p_2/(p_1 d)$ of the measure μ_1 [8, 28]. This reveals the utility of the transformation $F_1(s)$ in Equation (2.67), it reduces the $J=1$ case for $F(s)$ to the $J=0$ case for $F_1(s)$.

By our previous analysis, the values of $F_1(s)$ lie inside a circle $p_2/(p_1 d(s-\lambda))$, $-\infty \leq \lambda \leq \infty$. Similarly, the values of $E_1(s)$ lie inside a circle $p_1(d-1)/(p_2 d(s-\tilde{\lambda}))$, $-\infty \leq \tilde{\lambda} \leq \infty$. Since F and E are fractional linear in F_1 and E_1, respectively, these circles are transformed to the circles $C_1(\lambda)$ in the F-plane and $\tilde{C}_1(\tilde{\lambda})$ in the E-plane given by [28]

$$C_1(\lambda) = \frac{p_1(s-\lambda)}{s(s-\lambda-p_2/d)}, \quad \tilde{C}_1(\tilde{\lambda}) = \frac{p_2(s-\tilde{\lambda})}{s(s-\tilde{\lambda}-p_1(d-1)/d)}, \qquad -\infty \leq \lambda, \tilde{\lambda} \leq \infty. \quad (2.68)$$

In the σ^*-plane the intersection of these two circular regions is bounded by two circular arcs [28] corresponding to $0 \leq \lambda \leq (d-1)/d$ and $0 \leq \tilde{\lambda} \leq 1/d$ in (2.68).

The vertices of the region, $C_1(0) = p_1/(s-p_2/d)$ and $\tilde{C}(0) = p_2/(s-p_1(d-1)/d)$, are attained by the Hashin–Shtrikman geometries (spheres of all sizes of material 1 in the volume fraction p_1 coated with spherical shells of material 2 in the volume fraction p_2 filling all of $\mathbb{R}^d$, and vice versa), and lie on the arcs of the first order bounds [28]. While there are at least five points on the arc $C_1(\lambda)$ in (2.68) that are attainable by composite microstructures [54], the arc $\tilde{C}_1(\tilde{\lambda})$ in (2.68) violates [28] the interchange inequality $m(h)m(1/h) \geq 1$ [49, 66], which becomes an equality in two dimensions [56]. Consequently, the isotropic bounds in (2.68) are not optimal, but have been improved [53, 8] by incorporating the interchange inequality. When σ_1 and σ_2 are real and positive with $\sigma_1 \leq \sigma_2$, the region collapses to the interval

$$\sigma_1 + p_2 \left/ \left(\frac{1}{\sigma_2 - \sigma_1} + \frac{p_1}{d\sigma_1} \right) \right. \leq \sigma^* \leq \sigma_2 + p_1 \left/ \left(\frac{1}{\sigma_1 - \sigma_2} + \frac{p_2}{d\sigma_2} \right) \right., \qquad (2.69)$$

which are the Hashin–Shtrikman bounds.

The higher moments μ^n, for $n \geq 2$, depend on the $(n+1)$-point correlation functions of the medium [33] and have not be calculated in general. Although, the interchange inequality forces relations among them [55]. If the moments $\mu^0, \ldots, \mu^J$ are known, then the transformation F_1 in (2.67) can be iterated to produce an upper half plane function F_J with an integral representation, involving a positive measure μ_J which is supported on the interval $[0,1]$. As in the case where $J=1$, the first J moments of the measure μ determine only the mass μ_J^0 of the measure μ_J [28], and the function $F_J(s)$ can easily be extremized by the above procedure, and similarly for a function $E_J(s)$ associated with the moments $\eta^0, \ldots, \eta^J$. The resulting bounds form a nested sequence of lens-shaped regions [28].

3. Numerical results

In sections 2.2.2–2.2.4 we extended the ACM for representing transport in composites to the case of two-phase random media with finite lattice composite microstructure. This led to discrete, Stieltjes integral representations for the effective transport coefficients of such media, involving spectral measures associated with the random operators $M_i = \chi_i \Gamma \chi_i$ and $K_i = \chi_i \Upsilon \chi_i$, $i = 1, 2$. More specifically, we demonstrated in Section 2.2.2 that, in the finite lattice setting, these random operators are represented by random matrices. In Section 2.2.3, we provided a novel formulation of the ACM, which holds for both the matrix setting and the abstract linear operator setting discussed in sections 2.1 and 2.2.1. In Section 2.2.4 we utilized this novel formulation of the ACM to prove Theorem 2.1, which was stated in Section 2.2.2. The proof of this theorem establishes the existence of integral representations for the effective transport coefficients in the matrix setting, and demonstrates that the underlying spectral measures are given explicitly in terms of the eigenvalues and eigenvectors of the random matrices.

In this section, we utilize the mathematical framework described above to compute spectral measures and effective transport coefficients associated with the family of random bond lattices introduced in Section 2.2.2. In particular, we developed in Section 2.2.4 a numerically efficient projection method, summarized by equations (2.57)–(2.59), to facilitate such computations. Here, we employ this projection method to directly compute spectral measures and effective transport coefficients associated with this family of composites, which has various isotropic and anisotropic finite lattice composite microstructures.

In order to explore the relationship between the values of the effective transport coefficients and the associated bounds discussed in Section 2.3, we will focus on the diagonal components of the effective tensors and the underlying spectral measures, e.g., $\sigma_{kk}^* = \sigma_2 m_{kk}(h)$ and μ_{kk} for $k = 1, \ldots, d$. In this section, the values of the component conductivities σ_1 and σ_2 are taken to be that of the brine and pure ice phase, respectively, for a sample of sea ice measured at a frequency of 4.75GHz [4], with $\sigma_1 = 51.0741 + \imath 45.1602$ and $\sigma_2 = 3.07 + \imath 0.0019$, so that $s \approx -0.034 + \imath 0.032$. We stress that both the values of the effective complex conductivity σ_{kk}^* and resistivity ρ_{kk}^*, as well as the associated bounds, depend on the value of the contrast parameter $s = 1/(1 - \sigma_1/\sigma_2)$.

We now discuss our numerical method for computing spectral measures and effective transport coefficients in the matrix setting. Consider a two-phase random medium with finite lattice composite microstructure, as described by the matrix $\chi_1(\omega)$ defined in Equation (2.35), for $\omega \in \Omega$. From Equation (2.36), we see that the spectral measure μ_{kk}, $k = 1, \ldots, d$, for example, is an ensemble average of spectral measures $\mu_{kk}(\omega)$ associated with the matrices $M_1(\omega) = \chi_1(\omega) \Gamma \chi_1(\omega)$, for $\omega \in \Omega$. In particular, for fixed $\omega \in \Omega$, the measure $\mu_{kk}(\omega)$ is a weighted sum of δ-measures centered at the eigenvalues $\lambda_i(\omega)$ of $M_1(\omega)$, $i = 1, \ldots, N$, with weights $[\chi_1(\omega) Q_i(\omega) \hat{e}_k] \cdot \hat{e}_k$ involving the eigenvectors $\vec{u}_i(\omega)$ of $M_1(\omega)$ via $Q_i = \vec{u}_i \vec{u}_i^T$.

However, Equation (2.51) implies that the measure weights $[\chi_1(\omega) Q_i(\omega) \hat{e}_k] \cdot \hat{e}_k$ are identically zero for $i = 1, \ldots, N_0(\omega)$. This was used in Equation (2.59) to show that the measure $\mu_{kk}(\omega)$ depends only on the eigenvalues $\lambda_i^1(\omega)$, $i = 1, \ldots, N_1(\omega)$, and eigenvectors $\vec{u}_i^1(\omega)$ of the principle sub-matrix $\Gamma_1(\omega)$ of $\Pi(\omega) M_1(\omega) \Pi^T(\omega)$, introduced in Equation (2.48), and that the measure weights can be expressed more explicitly as $Q_i^1(\omega) \hat{e}_k^{\pi_1} \cdot \hat{e}_k^{\pi_1}$ with $Q_i^1 = \vec{u}_i^1 [\vec{u}_i^1]^T$. Consequently, for fixed $s \in \mathbb{C} \backslash [0, 1]$, the value of the effective complex conductivity $\sigma_{kk}^* = \sigma_2 (1 - F_{kk}(s))$ of the medium can be obtained by computing $\lambda_i^1(\omega)$ and $\vec{u}_i^1(\omega)$ for all $i = 1, \ldots, N_1(\omega)$ and each $\omega \in \Omega$. Since the computational cost of finding all the eigenvalues and eigenvectors of a $N \times N$ real-symmetric

matrix is $O(N^3)$ [23], this "projection method" makes the numerical computation of μ_{kk} and σ^*_{kk} much more efficient, especially for dilute systems where the size $N_1(\omega)$ of the matrix $\Gamma_1(\omega)$ satisfies $N_1(\omega) \ll N$ for all $\omega \in \Omega$.

For a random two-component bond lattice on $\mathbb{Z}^d_L$ with dimension d and size L, the cardinality $|\Omega|$ of the sample space Ω of geometric configurations is given by $|\Omega| = 2^N$, where $N = dL^d$. For large N, it becomes numerically expensive to compute the eigenvalues and eigenvectors of the matrix $\Gamma_1(\omega)$ for *every* $\omega \in \Omega$. In our numerical computations of the spectral measure μ_{kk}, for example, we instead used a reduced sample space $\Omega_0 \subset \Omega$ of randomly generated configurations of Ω. For each $\omega \in \Omega_0$, *all* of the eigenvalues and eigenvectors of the matrix $\Gamma_1(\omega)$ were computed using the MATLAB function *eig()*. We used lattice sizes $L = 60$ for $d = 2$ and $L = 10$ or $L = 15$ for $d = 3$ and typically averaged over $|\Omega_0| \sim 10^4$ – 10^5 geometric configurations.

In order to visually determine the behavior of the function $\mu_{kk}(\lambda) = \langle Q(\lambda)\hat{e}_k, \hat{e}_k \rangle_1$ underlying the spectral measure μ_{kk} for a given random lattice, we plot a histogram representation of $\mu_{kk}(\lambda)$ called the *spectral function*, which we will also denote by $\mu_{kk}(\lambda)$. We now describe how we computed this graphical representation of the measure μ_{kk}. First, the spectral interval $[0,1]$ was divided into R sub-intervals I_r, $r = 1,\ldots,R$, of equal length $1/R$. Second, for fixed r, we identified all of the eigenvalues that satisfy $\lambda^1_i(\omega) \in I_r$, for $i = 1,\ldots,N_1(\omega)$ and $\omega \in \Omega_0$. The assigned value of $\mu_{kk}(\lambda)$ at the midpoint λ of the interval I_r is the sum of the spectral weights $Q^1_i(\omega)\hat{e}^{\pi_1}_k \cdot \hat{e}^{\pi_1}_k$ associated with all such $\lambda^1_i(\omega) \in I_r$, normalized by $|\Omega_0|$. In our computations of the spectral functions, we typically used $R \sim 10^2$. As the system size increases, the eigenvalues become increasingly dense in the spectral interval $[0,1]$. For a large enough fixed system or for a random system averaged over many statistical realizations, the spectral functions $\mu_{kk}(\lambda)$, $k = 1,\ldots,d$, begin to resemble smooth curves, as shown in Figure 3.1.

In Figure 3.1(a), statistical realizations of the anisotropic 2D bond lattice are displayed for $L = 60$ and a volume (number) fraction $p_1 = 0.5$ of type-one bonds, with various values of p^k_1, $k = 1,2$, the volume fraction of type-one bonds in the positive k^{th} direction. The type-one bonds are colored black, and the largest connected cluster of type-one bonds has been re-colored grey. The type-two bonds are not visible. In Figure 3.1(b) and (c), we display the behavior of the spectral functions $\mu_{11}(\lambda)$ and $\mu_{22}(\lambda)$, respectively, as p^k_1 varies. In Figure 3.1(d), the computed values of the effective complex conductivities σ^*_{11} and σ^*_{22} are displayed along with the first order bounds of Equation (2.66) with $s = -0.034 + i0.032$. These bounds depend only on the mass $\mu^0_{kk} = dp^k_1$ of the measure μ_{kk} and the value of the contrast parameter $s = 1/(1 - \sigma_1/\sigma_2)$. Consistent with the symmetries of the model, these spectral functions and effective complex conductivities satisfy $\mu_{11}(\lambda) = \mu_{22}(\lambda)$ and $\sigma^*_{11} = \sigma^*_{22}$ for $p^1_1 = p^2_1$ (to numerical accuracy and statistical truncation).

We now consider the locally isotropic and statistically isotropic composite classes introduced in Section 2.2.2. In Figure 3.2, we display the behavior of the spectral functions and the effective complex conductivity and resistivity as a function of p_1 for locally isotropic random media with $L = 60$. Statistical realizations of the composite microstructure are displayed in Figure 3.2(a) with the same bond color scheme as that for Figure 3.1(a). The associated spectral functions $\mu_{11}(\lambda)$ displayed in Figure 3.2(b) exhibit a rich resonance structure for small values of p_1. These so called "geometric" resonances have been attributed [46] to the recurrence of local geometric structures called "fractal animals." Consistent with isotropy, the behavior of the spectral function $\mu_{22}(\lambda)$ is very similar to that of $\mu_{11}(\lambda)$ shown in Figure 3.2(b). The spectral functions $\mu_{kk}(\lambda)$, $k = 1,2$, were computed in [58] for the case of statistically isotropic random
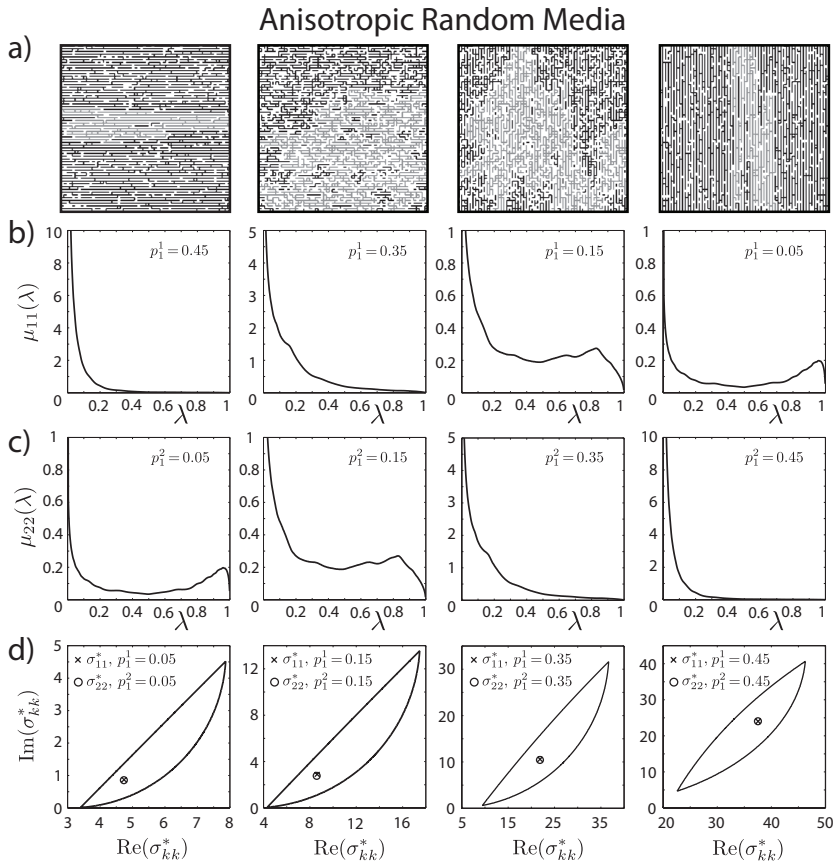
Anisotropic Random Media

FIG. 3.1. *Spectral measures and effective complex conductivities for anisotropic random media. Statistical realizations of the 2D square bond lattice for $p_1 = 0.5$ and various values of p_1^k, $k = 1, 2$, are displayed in (a). The type-one bonds are colored black, while the largest connected cluster of type-one bonds is colored grey. The corresponding spectral functions $\mu_{11}(\lambda)$ and $\mu_{22}(\lambda)$ are displayed in (b) and (c), respectively. The values of the effective complex conductivities σ_{11}^* and σ_{22}^* are displayed in (d) for $p_1^1 = p_1^2$ along with the first-order bounds for $s = -0.034 + \iota 0.032$. The computed spectral functions have been rescaled so that the area under the graph is the measure mass $\mu_{kk}^0 = d p_1^k$.*

FIG. 3.2. *Spectral measures and effective complex conductivities and resistivities for locally isotropic random media. Realizations of the two-dimensional lattice model are displayed in (a). The type-one bonds are colored black, while the largest connected cluster of type-one bonds is colored grey. The corresponding spectral functions $\mu_{11}(\lambda)$ are displayed in (b). The values of the effective complex conductivity σ_{kk}^* and resistivity ρ_{kk}^*, $k = 1, 2$, are displayed in (c) and (d), respectively, along with the corresponding isotropic bounds for $s = -0.034 + \iota 0.032$. The computed spectral functions have been rescaled so that the area under the graph is the measure mass $\mu_{11}^0 = p_1$.*

media. They look very similar to $\mu_{11}(\lambda)$ in Figure 3.2(b). In Section 2.2.2 we noted that, in *two dimensions*, the projection matrices Γ and Υ are related by $\Upsilon = R^T \Gamma R$, where R is $90°$ rotation matrix. As a consequence, the spectral functions $\kappa_{kk}(\lambda)$, $k = 1, 2$, for 2D locally and statistically *isotropic* random media look very similar to $\mu_{11}(\lambda)$ displayed in Figure 3.2(b). In Figure 3.2(c) and (d), the values of the effective complex conductivities σ_{kk}^* and resistivities ρ_{kk}^*, $k = 1, 2$, are displayed, respectively, along with the isotropic bounds from Equation (2.68) for $s = -0.034 + \iota 0.032$. Consistent with
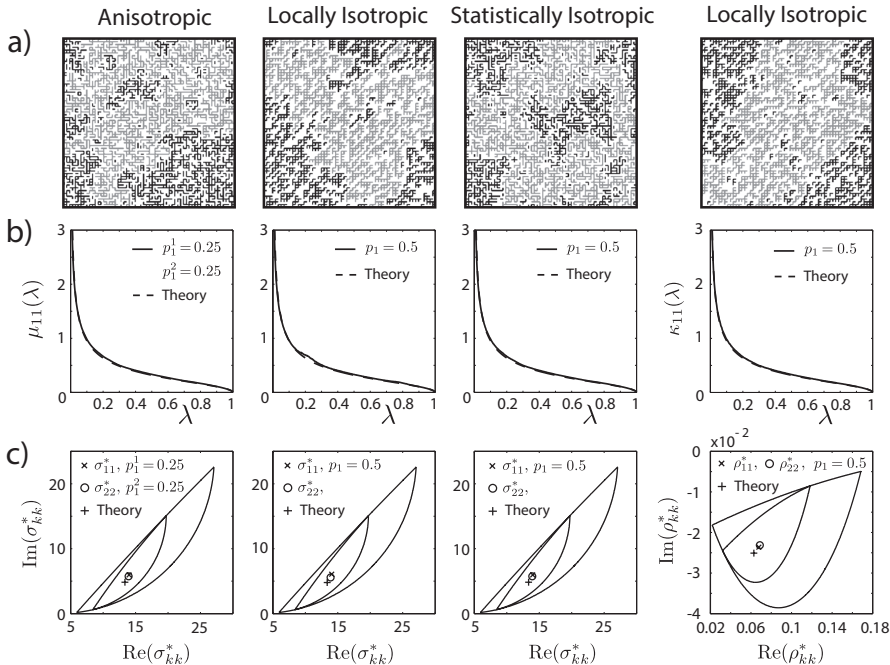
FIG. 3.3. *Statistically self-dual random media. Realizations of various 2D lattice models are displayed in (a). The type-one bonds are colored black, while the largest connected cluster of type-one bonds is colored grey. The corresponding spectral function $\mu_{11}(\lambda)$ or $\kappa_{11}(\lambda)$ is displayed in (b). The values of the effective complex conductivity σ_{11}^* or resistivity ρ_{11}^*, for $s = -0.034 + \imath 0.032$, are displayed in (c). Also displayed in (b) is the theoretical prediction for infinite, self-dual composite microstructures. The theoretical prediction for the value of the effective complex conductivity or resistivity, as well as the first-order and isotropic bounds, are also displayed in (c). The computed spectral functions have been rescaled so that the area under the graph is the measure mass $\mu_{11}^0 = p_1$.*

isotropy, we have that $\sigma_{11}^* = \sigma_{22}^*$ and $\rho_{11}^* = \rho_{22}^*$ (to numerical accuracy and statistical truncation) and $\sigma_{kk}^* = 1/\rho_{kk}^*$ to a relative error $|\sigma_{kk}^* - 1/\rho_{kk}^*|/|\sigma_{kk}^*| \lesssim 10^{-2}$.

In the infinite lattice setting, the statistically and locally isotropic composite microstructures are statistically self-dual [56] for $d = 2$ and $p_1 = 0.5$. Note that the class of anisotropic random media for the special case of $p_1^k = p_1/d$, for all $k = 1, \ldots, d$, is also statistically isotropic and self-dual for $d = 2$ and $p_1 = 0.5$. For such systems, the spectral measures and effective transport coefficients may be explicitly calculated [56], e.g., $\mathrm{d}\mu_{kk}(\lambda) = (\sqrt{(1-\lambda)/\lambda})(\mathrm{d}\lambda/\pi)$ and $\sigma_{kk}^* = \sqrt{\sigma_1 \sigma_2}$, $k = 1, \ldots, d$. In particular, the spectral measure μ_{kk} is absolutely continuous with respect to the Lebesgue measure [27], with density $\mu_{kk}(\lambda) = (\sqrt{(1-\lambda)/\lambda})/\pi$.

These theoretical predictions, holding for infinite systems, are displayed in Figure 3.3 along with our computations of spectral functions and effective transport coefficients for a finite system size $L = 60$. Statistical realizations of the finite lattice microstructures are displayed in Figure 3.3(a), with the same bond color scheme as that for Figure 3.1(a). It is remarkable that even for the finite system size $L = 60$, the computed spectral functions displayed in Figure 3.3(b) agree quite well with the theoretical duality prediction, which holds for infinite lattices. The anomalous difference between the theory and the numerical computation, seen in Figure 3.3(b) for locally isotropic random media, becomes less prominent as L increases and is virtually absent for $L = 100$. In Figure 3.3(c), the computed values of the effective transport coefficients

are displayed along with the duality prediction and the first-order and isotropic bounds from equations (2.66) and (2.68), respectively, with $s = -0.034 + \imath 0.032$. The computed values of the effective transport coefficients are in excellent agreement with that of the duality prediction, which holds for infinite systems. The deviation in the computed values of the effective parameters, relative to the duality prediction, is typically $\lesssim 10^{-2}$ for $L = 60$ and decreases with increasing L.

The integral representation displayed in Equation (2.36) is also valid for the effective transport coefficients of two-phase random media with *three-dimensional*, finite lattice composite microstructure. We now discuss our computations of spectral measures and effective transport coefficients for such random media. Typical of numerical simulations associated with three-dimensional systems, there are fundamental numerical challenges that arise when extending our spectral measure computations to 3D composite microstructures. These challenges are consequences of the size $N = dL^d$ of the matrices $M_1 = \chi_1 \Gamma \chi_1$ and $K_1 = \chi_1 \Upsilon \chi_1$, which rapidly increases with system size L when $d = 3$.

One challenge is the numerical cost of computing *all* of the eigenvalues and eigenvectors of a $N \times N$ real-symmetric matrix, which is $O(N^3)$ [23]. However, for the statistically self-dual composite microstructures discussed above, the deviation in the computed values of the effective parameters for $L = 15$, relative to the theoretical duality prediction for the *infinite lattice*, is typically $\lesssim 10^{-1}$. This indicates that the computations of the effective transport coefficients are reasonably accurate even for small system sizes L. Moreover, for random media with geometric configurations that are statistically independent of each other, the numerical computations of the associated eigenvalues and eigenvectors can be performed in parallel.

Another challenge associated with a large matrix size N, is the numerical accuracy of the computations. We computed the matrices $\Gamma = \nabla(\Delta^{-1})\nabla^T$ and $\Upsilon = C(C^T C)^{-1}C^T$ using the MATLAB *mldivide* function $A \backslash B$, i.e., $\Gamma = \nabla(\Delta \backslash \nabla^T)$ and $\Upsilon = C[(C^T C)\backslash C^T]$. Since ∇ and C are *sparse* matrices with *integer elements*, the matrices Γ and Υ were efficiently computed using MATLAB's sparse architecture, which also reduces roundoff error in the computations. The numerical accuracy of these "matrix inversions" depends on the matrix condition number $\mathcal{K}(A)$, for $A = \Delta, C^T C$. The matrix A is said to be *well-conditioned* when $\mathcal{K}(A)$ is small and *ill-conditioned* when $\mathcal{K}(A)$ is large. One must always expect to "lose $\log_{10}\mathcal{K}(A)$ digits" of accuracy in computing the solution, except under very special circumstances [74]. The numerical accuracy of the eigenvalue problem for the matrices $M_1 = \chi_1 \Gamma \chi_1$ and $K_1 = \chi_1 \Upsilon \chi_1$ is determined by the associated eigenvalue condition numbers, which are the reciprocals of the cosines of the angles between the left and right eigenvectors. Large eigenvalue condition numbers of a symmetric matrix A imply that it is near a matrix with multiple eigenvalues, while eigenvalue condition numbers ≈ 1 imply that the eigenvalue problem is well-conditioned.

We now discuss the condition numbers of the matrices Δ and $C^T C$ for the system sizes considered in our computations. Recall for $d = 2$ that $C^T C = \Delta$. In this 2D case, $\mathcal{K}(\Delta) \sim 10^3$ for $L = 60$ and $L = 100$. In the 3D case $C^T C \neq \Delta$, and $\mathcal{K}(\Delta) \sim 10^1$ for $L = 10$ and $\sim 10^2$ for $L = 15$, while $\mathcal{K}(C^T C) \sim 10^6$ for $L = 10$ and $\sim 10^7$ for $L = 15$. These condition numbers were estimated using the MATLAB function *condest()*. The eigenvalue condition numbers for the matrices $M_1 = \chi_1 \Gamma \chi_1$ and $K_1 = \chi_1 \Upsilon \chi_1$ were computed using the MATLAB function *condeig()*. They are all ≈ 1 for the system sizes considered, indicating that the associated eigenvalue problems are well-conditioned. In summary, within the double precision architecture of MATLAB with a *machine epsilon* $\epsilon \sim 10^{-16}$, for the system sizes L considered, the spectral measure computations associated with the matrices M_1 and K_1 are well-conditioned for $d = 2$. The spectral measure
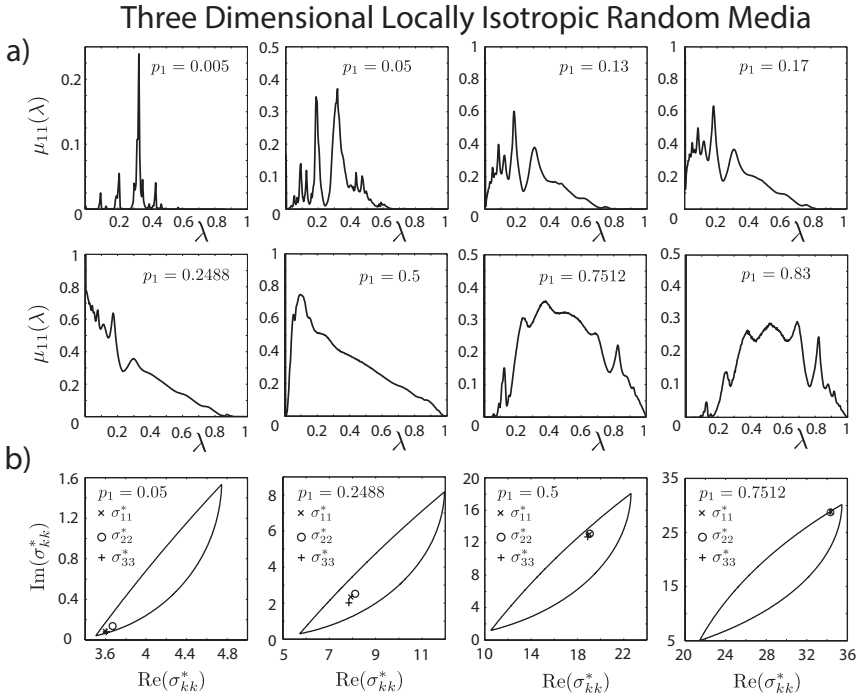
FIG. 3.4. *Spectral measures and effective conductivities for 3D locally isotropic random media. The spectral function $\mu_{11}(\lambda)$ is displayed in (a) for various volume fractions p_1 of type-one bonds. Computed values of the effective complex conductivity σ_{kk}^*, $k = 1, \ldots, d$, are displayed in (b) along with the isotropic bounds for $s = -0.034 + \imath 0.032$. The spectral functions have been rescaled so that the area under the graph is the measure mass $\mu_{11}^0 = p_1$.*

computations associated with the matrix M_1 are also well-conditioned for $d = 3$, while those of the matrix K_1 are relatively ill-conditioned for $d = 3$. The problem of finding an appropriate *preconditioner* for the matrix $C^T C$ in the 3D case is a topic of current work.

Displayed in Figure 3.4 are computations of spectral functions and effective complex conductivities for three-dimensional locally isotropic random media with $L = 15$. Like its 2D counterpart, the spectral function $\mu_{11}(\lambda)$ displayed in Figure 3.4(a) has a rich resonant structure for small values of p_1. Consistent with isotropy, the behavior of the spectral functions $\mu_{kk}(\lambda)$ for $k = 2, 3$ are very similar to that of $\mu_{11}(\lambda)$ shown in Figure 3.4(a). The spectral functions $\mu_{kk}(\lambda)$, $k = 1, 2, 3$, were computed in [58] for the case of statistically isotropic random media. They look very similar to $\mu_{11}(\lambda)$ in Figure 3.4(a). In Figure 3.4(b), the values of the effective complex conductivities σ_{kk}^*, $k = 1, 2, 3$, are displayed along with the isotropic bounds from Equation (2.68) for $s = -0.034 + \imath 0.032$. Consistent with isotropy, $\sigma_{jj}^* = \sigma_{kk}^*$ for all $j, k = 1, 2, 3$ (to numerical accuracy and statistical truncation).

Displayed in Figure 3.5 are computations of the spectral function $\kappa_{11}(\lambda)$ associated with the effective complex resistivity ρ_{11}^* for 3D locally isotropic random media with various values of p_1. In order to increase the numerical stability of the computation, we reduced the system size from $L = 15$ to $L = 10$. The limited numerical accuracy in the computation of $\Upsilon = C(C^T C)^{-1} C^T$, which is then propagated to the eigenvalue problem for $K_1 = \chi_1 \Upsilon \chi_1$, seems to have a smoothing effect, and there are no prominent reso-
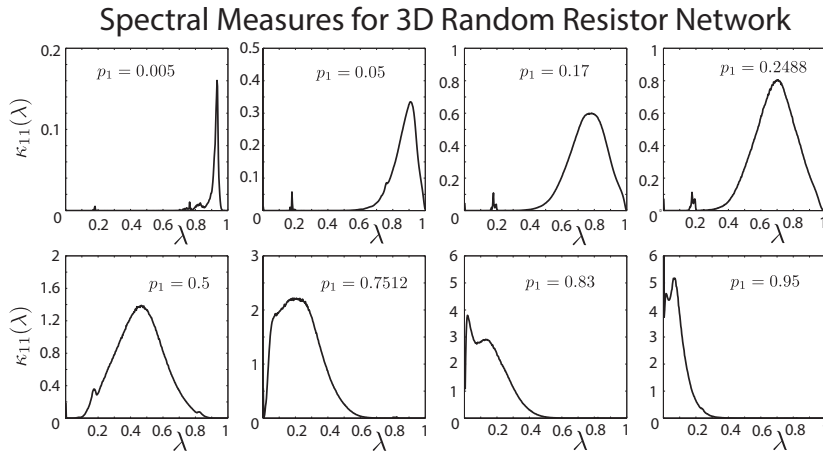
Spectral Measures for 3D Random Resistor Network

FIG. 3.5. *Spectral measures for 3D locally isotropic random media. The spectral function $\kappa_{11}(\lambda)$ is displayed for various volume fractions p_1 of type-one bonds. They have been rescaled so that the area under the graph is the measure mass $\kappa_{11}^0 = p_1$.*

nances in the spectral functions for small values of p_1. A smoothing effect is typical for regularization of ill-posed inverse problems for the reconstruction of spectral measures [13]. Consistent with isotropy, $\kappa_{11}(\lambda) \approx \kappa_{33}(\lambda)$ and $\rho_{11}^* \approx \rho_{33}^*$. Although, due to the limited accuracy of the computations, the behavior of $\kappa_{22}(\lambda)$ and the value of ρ_{22}^* is significantly different from that of the other two components.

We now discuss the gap behavior of the spectral measures [58, 46] and the governing role that it plays in critical transitions exhibited by the integral representations for the effective transport coefficients [58, 30]. In the infinite lattice setting, the isotropic composite microstructures discussed in this section are examples of lattice percolation models [70, 73], which are parameterized by the volume fraction $p_1 = 1 - p_2$ of the constituents. In these lattice percolation models, the bonds are open with probability p_2, say, and closed with probability p_1. Connected sets of open bonds are called open clusters. The average cluster size grows as p_2 increases, and there is a critical probability p_c, $0 < p_c < 1$, called the *percolation threshold*, where an infinite cluster of open bonds first appears. For the two-dimensional lattice percolation model, $p_c = 0.5$, and in three-dimensions $p_c \approx 0.2488$ [70, 73].

Now consider transport through the associated RRN, where the bonds are assigned electrical conductivities σ_1 with probability p_1 and σ_2 with probability p_2. The effective conductivity $\sigma^*(p_1, h)$, for example, exhibits two types of critical behavior as $h = \sigma_1/\sigma_2 \to 0$. First, when $\sigma_1 = 0$ and $0 < |\sigma_2| < \infty$, $\sigma^*(p_1, 0) = 0$ for $p_1 > 1 - p_c$ while $|\sigma^*| > 0$ for $p_1 < 1 - p_c$. Second, when $|\sigma_2| \to \infty$ and $0 < |\sigma_1| < \infty$, $|\sigma^*(p_1, 0)| \to \infty$ as $p_1 \to 1 - p_c^+$. Since $s = 1/(1-h)$ and $t = 1 - s$, we see from Equation (2.12) that the associated critical behavior of the integral representations for $m_{kk}(p_1, h) = \sigma^*(p_1, h)/\sigma_2$ and $w_{kk}(p_2, z) = \sigma^*(p_2, z)/\sigma_1$ depends, in turn, on the behavior of the spectral measures $\mu_{kk}(p_1)$ and $\alpha_{kk}(p_2)$ at the spectral endpoints $\lambda = 0, 1$.

Consider the behavior of the spectral measure μ_{11} at the spectral endpoints $\lambda = 0, 1$ for the 2D lattice percolation model. In figures 3.2(b) and 3.3(b) we see that, as p_1 increases from zero and the system becomes increasingly connected, gaps in the spectral function $\mu_{11}(\lambda)$ at the spectral endpoints $\lambda = 0, 1$ shrink and then vanish symmetrically at a value of $p_1 = p_c = 0.5$. The graphs of these spectral functions indicate that the
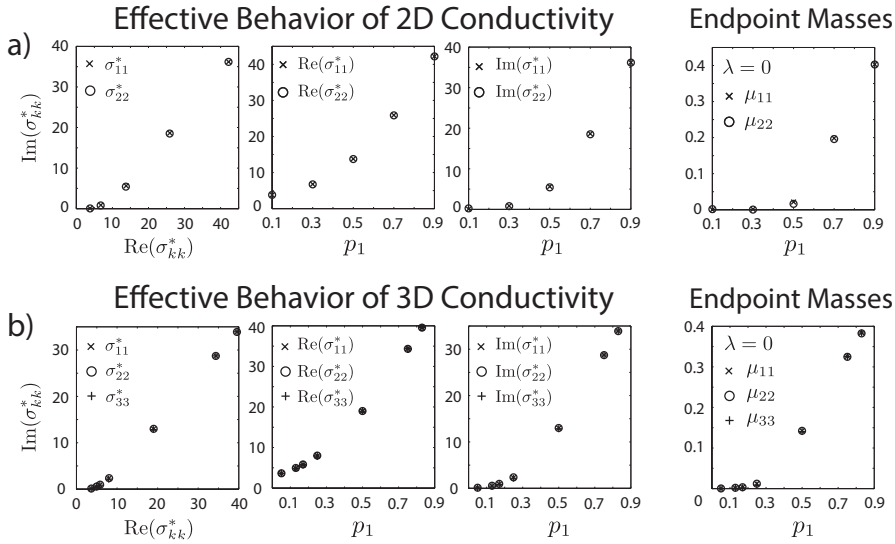
FIG. 3.6. *Behavior of effective complex conductivities and measure endpoint masses. The values of the effective complex conductivity σ_{kk}^*, for $k=1,\dots,d$ and $s=-0.034+\imath 0.032$, and the mass of the spectral measure μ_{kk} at $\lambda=0$ are displayed as a function of volume fraction p_1 for 2D (a) and 3D (b) locally isotropic random resistor network.*
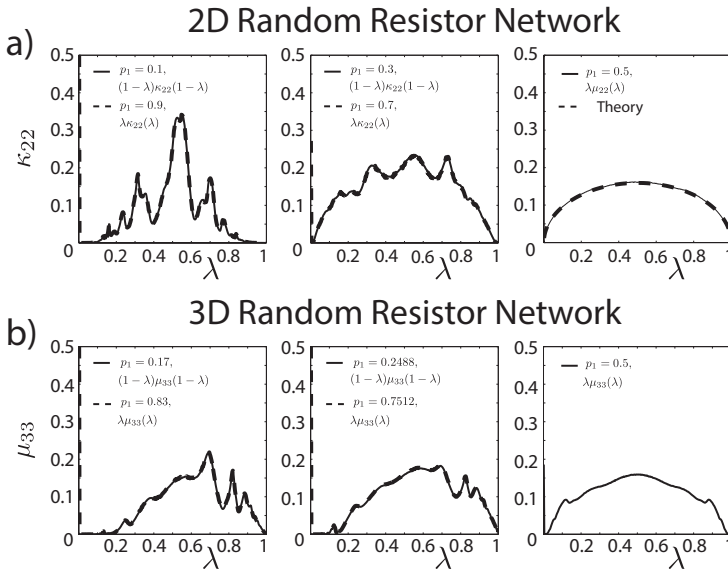

FIG. 3.7. *Spectral measure symmetries. Transformations of the computed spectral functions for 2D (a) and 3D (b) random resistor networks, for various values of the volume fraction p_1. The spectral functions have been rescaled so that the area under the graph is the measure mass.*

vanishing of the spectral gaps leads to a buildup in the mass of the measure at $\lambda=0$, while the mass of the measure is approximately zero for $\lambda=1$, i.e., $\mu_{11}(1)\approx0$. Moreover, as p_1 increases beyond the percolation threshold p_c, the mass of the measure at $\lambda=1$ remains approximately zero, while the buildup of the measure mass at $\lambda=0$ *persists and grows.*

Now consider the behavior of the spectral measures μ_{11} and κ_{11} at the spectral endpoints $\lambda=0,1$ for the 3D lattice percolation model. In Figure 3.4(a), we see as p_1 increases from zero and approaches the percolation threshold $p_c \approx 0.2488$, a spectral gap about $\lambda=0$ shrinks and then vanishes, leading to a buildup in the mass of the measure μ_{11} at $\lambda=0$ for $p_1=p_c$. As p_1 increases beyond p_c, the mass of μ_{11} at $\lambda=0$ continues to grow, while a spectral gap at $\lambda=1$ shrinks and then vanishes for $p_1=1-p_c \approx 0.7512$, with $\mu_{11}(1)\approx 0$. The spectral function $\kappa_{11}(\lambda)$ displayed in Figure 3.5 has an analogous transitional behavior. In particular, as p_1 increases from zero and approaches the percolation threshold $p_c \approx 0.2488$, a spectral gap about $\lambda=1$ shrinks and then vanishes, with $\mu_{11}(1)\approx 0$. As p_1 increases beyond p_c and approaches $1-p_c \approx 0.7512$, a spectral gap about $\lambda=0$ shrinks and vanishes, leading to a buildup in the mass of the measure κ_{11} at $\lambda=0$. Since $t=1-s$, it is consistent that the roles of the spectral endpoints for κ_{11} have switched from that of μ_{11}.

For finite lattice systems, the existence of gaps in the spectrum of μ_{11} about $\lambda=0,1$ for $p_1 \ll 1$, as well as their collapse as $p_1 \to 1$, is a direct consequence [58] of the projective nature of the matrices χ_1 and Γ. However, it has been argued for *infinite* lattice percolation models that the spectrum of μ_{11} extends all the way to the spectral endpoints $\lambda=0,1$, with exponentially decaying *Lifshitz tails* for all $0<p_1 \ll 1$. The detailed nature of the Lifshitz tails was numerically verified in [46] for the finite, 2D lattice percolation model for $p_1=0.05, 0.1, 0.15,$ and 0.2, demonstrating that this behavior of μ_{11} is present even in the finite lattice setting. The presence of these Lifshitz tails in μ_{11} explains the presence of measure masses near $\lambda=0$ for $p_1<p_c$ in figures 3.2 and 3.4, shown as vertical lines in the spectral function $\mu_{11}(\lambda)$ near $\lambda=0$.

Displayed in Figure 3.6 is the behavior of the effective complex conductivity σ_{kk}^* and the mass of the measure μ_{kk} concentrated at $\lambda=0$, for $k=1,\ldots,d$, as a function of volume fraction p_1 for the 2D (a) and 3D (b) locally isotropic lattice percolation models discussed in figures 3.2–3.4. It can be seen in Figure 3.6 that a very small fraction of the measure mass is concentrated at $\lambda=0$ for $p_1<p_c$, where $p_c=0.5$ for 2D and $p_c \approx 0.2488$ for 3D. However, as p_1 surpasses p_c, a significant amount of the measure mass becomes concentrated at the spectral endpoint $\lambda=0$. This δ-function behavior in the measure leads to large changes in the value of effective complex conductivity σ_{kk}^* as the volume fraction p_1 surpasses p_c. The computed mass of μ_{kk} concentrated at $\lambda=1$ is $\lesssim 10^{-30}$ for all values of p_1 considered, both in the 2D and 3D cases.

The gap behavior of the spectral measures discussed above is consistent with Equation (2.14), which holds for general stationary random media in the infinite setting [58] and consequently holds for percolation models of such media. This equation characterizes the percolation transition with the formation of delta components in the spectral measures at the spectral endpoints $\lambda=0,1$, *precisely* at $p_1=p_c$ and $p_1=1-p_c$. More specifically, the weights $m_{kk}(0)$ and $w_{kk}(0)$, $k=1,\ldots,d$, of the delta components at $\lambda=1$ and $\lambda=0$ in (2.14) have the following behavior. When $\sigma_1=0$ ($h=0$), the function $m_{kk}(0)=m_{kk}(p_1,0)$ increases from zero as p_1 surpasses $1-p_c$. Similarly, when $\sigma_2=0$ ($z=0$), the function $w_{kk}(0)=w_{kk}(p_2,0)$ increases from zero as p_1 surpasses p_c. This demonstrates that global connectedness of the system is encoded in the absence/presence of these delta components in the measure. For insulator/conductor or conductor/superconductor systems, this behavior in the spectral endpoints of the measures leads to critical behavior in the effective conductivity [58, 30].

Equation (2.14), which holds for infinite systems, also provides a relationship between the measures $\mu_{kk}(p_1)$ and $\alpha_{kk}(p_2)$, and the measures $\kappa_{kk}(p_1)$ and $\eta_{kk}(p_2)$. In Figure 3.7 we demonstrate that this relationship between the spectral measures persists

in the finite lattice setting. Displayed in Figure 3.7(a) are graphs of transformations of the spectral function $\kappa_{22}(\lambda)$ for the 2D lattice percolation model. In particular, the graph of the function $(1-\lambda)\kappa_{22}(1-\lambda)$ is displayed for volume fractions $p_1 = 0.1$, 0.3, and 0.5, along with $\lambda\kappa_{22}(\lambda)$ for volume fractions $1-p_1 = 0.9$, 0.7, and 0.5. Similarly, in Figure 3.7(b) the graphs of $(1-\lambda)\mu_{33}(1-\lambda)$ and $\lambda\mu_{33}(\lambda)$ are displayed for the 3D lattice percolation model with various values of p_1 and $1-p_1$, respectively. The graphs of the transformed spectral functions are virtually identical except for a "δ-function" at $\lambda = 0$, in excellent agreement with (2.14). We conclude this section by noting that, despite the lack of numerical accuracy in our computations of the spectral function $\kappa_{kk}(\lambda)$ for 3D finite lattice composite microstructures, the functions $(1-\lambda)\kappa_{kk}(p_1, 1-\lambda)$ and $\lambda\kappa_{kk}(p_2, \lambda)$ are also virtually identical, other than a singularity at $\lambda = 0$.

4. Conclusion

In sections 2.1 and 2.2.1, we reviewed and extended the ACM for representing transport in two-phase random media, for the *infinite* continuum and lattice settings, respectively. This method provides the Stieltjes integral representations displayed in Equation (2.12) for the effective transport coefficients of such composite media, which involve spectral measures associated with the self-adjoint random operators $M_i = \chi_i \Gamma \chi_i$ and $K_i = \chi_i \Upsilon \chi_i$. Here, χ_i is the characteristic function for material phase $i = 1, 2$, and the operators $\Gamma = \vec{\nabla}(\Delta^{-1})\vec{\nabla}\cdot$ and $\Upsilon = -\vec{\nabla}\times(\Delta^{-1})\vec{\nabla}\times$ act as projectors onto curl-free and divergence-free fields, respectively.

In Section 2.2.2, we developed the ACM for representing transport in two-phase random media with *finite* lattice composite microstructure, yielding discrete Stieltjes integral representations for the effective transport coefficients of such media, displayed in Equation (2.36) of Theorem 2.1, which is a key theoretical contribution of this work. We accomplished this by developing a unified formulation of the ACM in Section 2.2.3 that is equivalent to the original formulation [33], and holds for both the finite lattice setting and the infinite, continuum and lattice settings. We also provided a projection method for numerically efficient, rigorous computation of spectral measures and effective parameters for composite media with finite lattice composite microstructure. This projection method is summarized by equations (2.57)–(2.59). In this finite lattice case, the operators χ_i, Γ, and Υ are represented by real-symmetric projection matrices, and the spectral measures of the associated real-symmetric random matrices M_i and K_i are given explicitly in terms of their eigenvalues and eigenvectors, as displayed in Equation (2.36).

In Section 2.2.2, following the statement of Theorem 2.1, we introduced three families of locally isotropic, statistically isotropic, and anisotropic random media with finite lattice composite microstructure. In Section 3, we employed the projection method to compute the spectral measures and effective parameters associated with these families of random media. To our knowledge, this is the first time that the spectral measures η_{kk} and κ_{kk} underlying the effective complex resistivity ρ_{kk}^* have been computed for such composite microstructures. These computations not only demonstrate several important properties of the spectral measures and effective parameters, but they also serve as a consistency check to the theory developed here.

The computed spectral functions and effective complex parameters for anisotropic random media displayed in Figure 3.1 are consistent with the symmetries of the model. Consistent with general theory [56], our computations of the effective parameters for isotropic random media satisfy $\sigma_{kk}^* = 1/\rho_{kk}^*$, $k = 1, \ldots, d$ (to numerical accuracy and statistical truncation). Moreover, the computed spectral functions and effective parameters are consistent with isotropy and satisfy $\mu_{jj}(\lambda) = \mu_{kk}(\lambda)$ and $\sigma_{jj}^* = \sigma_{kk}^*$, for example, for

all $j,k=1,\ldots,d$ (to numerical accuracy, finite size effects, and statistical truncation). Figure 3.3 demonstrates that the projection method accurately computes the spectral measures and effective parameters for statistically self-dual composite microstructures. Furthermore, Figure 3.7 shows that the computed spectral measures are in excellent agreement with Equation (2.14), which holds for general stationary two-phase random media [58].

The self-consistent mathematical framework developed here helps lay the groundwork for studies in the effective transport properties of a broad range of important composites, such as electrorheological fluids [57], multiscale sea ice structures, and bone [32]. Remarkably, the ACM has also been adapted to provide Stieltjes integral representations for effective transport coefficients underlying a wide variety of transport processes, such as: the effective diffusivity for steady [50, 2] and time-dependent [3] fluid velocity fields, the effective complex permittivity for uniaxial polycrystalline media [5, 37], and the effective elastic moduli of two-phase elastic composites [60, 61]. The Golden-Papanicolaou formulation of the ACM has been pivotal in the development of these mathematical frameworks, and in the understanding of these important transport processes.

Appendix A. The spectral theorem. In equations (2.12) and (2.36) of sections 2.1 and 2.2.2, we display integral representations for the functions $F_{jk}(s)$, $G_{jk}(t)$, $E_{jk}(s)$, and $H_{jk}(t)$, $j,k=1,\ldots,d$, involving spectral measures μ_{jk}, α_{jk}, η_{jk}, and κ_{jk}, respectively, which are associated with the self-adjoint random operators $M_i=\chi_i\Gamma\chi_i$ and $K_i=\chi_i\Upsilon\chi_i$, $i=1,2$. In this section, we discuss the spectral theorem as it pertains to the ACM, which provides the existence of these Stieltjes integral representations. The abstract, bounded linear self-adjoint operator case [63, 72] associated with the infinite, continuum and lattice settings is discussed in Section A.1, while the real-symmetric matrix case [38, 69] associated with the finite lattice setting is discussed in Section A.2. Since the formulations associated with each of the operators $M_i=\chi_i\Gamma\chi_i$ and $K_i=\chi_i\Upsilon\chi_i$, $i=1,2$, are analogous, we will focus on that for the operator $M_1=\chi_1\Gamma\chi_1$. Also, in Section 2.2.3 we provided a novel formulation of the ACM involving the operator M_1, which is equivalent to the original formulation [33] involving the operator $\Gamma\chi_1$, and holds for both the finite lattice setting and the infinite. Due to this unification, we will focus on the formulation of the ACM associated with the operator M_1.

A.1. Infinite continuum and lattice settings.   In this section, we review the spectral theorem as it pertains to the ACM for the infinite, continuous and lattice settings. Consider the Hilbert space $\mathscr{H}_\times$ defined in Equation (2.2). Now, define the Hilbert space $\mathscr{H}_0=\mathscr{H}_\times\cup\mathbb{C}^d$ by

$$\mathscr{H}_0=\left\{\vec{Y}\in\mathscr{H}\mid\vec{\nabla}\times\vec{Y}=0\text{ weakly}\right\}, \tag{A.1}$$

where $\vec{\nabla}\times\vec{Y}=0$ means that $L_iY_j-L_jY_i=0$ for all $i,j=1,\ldots,d$. In other words, $\mathscr{H}_0$ is the Hilbert space $\mathscr{H}_\times$ with the constant fields $\mathbb{C}^d$ included. Equip $\mathscr{H}_0$ with the $\mathscr{H}$-inner-product weighted by the characteristic function χ_1, which we denote by $\langle\cdot,\cdot\rangle_1$. In the infinite, continuum and lattice settings, the characteristic function acts *pointwise* on the underlying vector space, $\mathbb{R}^d$ or $\mathbb{Z}^d$, and it is therefore a self-adjoint operator on $\mathscr{H}_0$. Clearly, it is also a linear projection operator satisfying $\langle\chi_1\vec{\xi},\vec{\zeta}\rangle=\langle\chi_1^2\vec{\xi},\vec{\zeta}\rangle$ for all $\vec{\xi},\vec{\zeta}\in\mathscr{H}_0$, and is therefore bounded on $\mathscr{H}_0$ with operator norm $\|\chi_1\|\le1$.

On $L^2(\Omega,P)$, the linear operator Δ^{-1} is self-adjoint [69]. For all $\vec{\xi}\in\mathscr{H}_0$ we have $\vec{\nabla}\cdot\vec{\xi}\in L^2(\Omega,P)$, and for all $\zeta\in L^2(\Omega,P)$ we have $\|\vec{\nabla}\Delta^{-1}\zeta\|<\infty$, where $\|\cdot\|$ denotes

the norm induced by the $\mathscr{H}$-inner-product. It follows that the linear operator $\Gamma = \vec{\nabla}(\Delta^{-1})\vec{\nabla}\cdot$ is bounded on $\mathscr{H}_0$. Integration by parts then establishes that Γ is self-adjoint on $\mathscr{H}_0$ [33]. It is also clear that Γ is a projection operator satisfying $\langle \Gamma\vec{\xi},\vec{\zeta}\rangle = \langle \Gamma^2\vec{\xi},\vec{\zeta}\rangle$ for all $\vec{\xi},\vec{\zeta}\in\mathscr{H}_0$, with operator norm $\|\Gamma\|\leq 1$.

It follows that $M_1 = \chi_1\Gamma\chi_1$ is a bounded linear self-adjoint operator on the Hilbert space $\mathscr{H}_0$, with operator norm $\|M_1\|\leq 1$ [63, 72]. The spectrum Σ of the self-adjoint operator M_1 is real-valued and the spectral radius of M_1 is equal to its operator norm [63], which implies that $\Sigma\subseteq[-1,1]$. However, since χ_1 and Γ are self-adjoint projection operators on $\mathscr{H}_0$, we have $\langle \chi_1\Gamma\chi_1\vec{\xi},\vec{\xi}\rangle = \langle \Gamma\chi_1\vec{\xi},\Gamma\chi_1\vec{\xi}\rangle = \|\Gamma\chi_1\vec{\xi}\|^2 \geq 0$ for all $\vec{\xi}\in\mathscr{H}_0$. This implies that M_1 is also a positive operator, which implies that its spectrum satisfies $\Sigma\subseteq[0,\infty)$ [72]. Consequently, the spectrum Σ of M_1 satisfies $\Sigma\subseteq[0,1]$.

Since $\Sigma\subseteq[0,1]$, the spectral theorem for bounded linear self-adjoint operators in Hilbert space [72] states that there is a one-to-one correspondence between the operator M_1 and a family of self-adjoint projection operators $\{Q(\lambda)\}_{\lambda\in[0,1]}$ — the resolution of the identity — that satisfies $\lim_{\lambda\to 0}Q(\lambda) = 0$ and $\lim_{\lambda\to 1}Q(\lambda) = I$, where 0 and I are the null and identity operators on $\mathscr{H}_0$. Furthermore, for all $\vec{\xi},\vec{\zeta}\in\mathscr{H}_0$, the function of λ defined by $\mu_{\xi\zeta}(\lambda) = \langle Q(\lambda)\vec{\xi},\vec{\zeta}\rangle_1$ is strictly increasing and of bounded variation, and therefore has a Stieltjes measure $\mu_{\xi\zeta}$ associated with it [71, 72, 27]. The spectral theorem also states [72], for all complex valued functions $f,g\in L^2(\mu_{\xi\zeta})$, there exists linear operators denoted by $f(M_1)$ and $g(M_1)$ which are defined in terms of the bilinear functional $\langle f(M_1)\vec{\xi}, g(M_1)\vec{\zeta}\rangle_1 = \langle f(M_1)\chi_1\vec{\xi}\cdot g(M_1)\vec{\zeta}\rangle$. In particular, this functional has the following integral representation involving the Stieltjes measure $\mu_{\xi\zeta}$:

$$\langle f(M_1)\vec{\xi}, g(M_1)\vec{\zeta}\rangle_1 = \int_0^1 f(\lambda)\bar{g}(\lambda)\mathrm{d}\mu_{\xi\zeta}(\lambda), \quad \mu_{\xi\zeta}(\lambda) = \langle Q(\lambda)\vec{\xi},\vec{\zeta}\rangle_1, \qquad \text{(A.2)}$$

where the integration is over the spectrum Σ of M_1 [63, 72] and we have taken the dot-product $\vec{\xi}\cdot\vec{\zeta}$ on $\mathbb{C}^d$ to be complex conjugated in the *second* argument with $\bar{g}$ denoting the complex conjugate. Setting $f(\lambda) = (s-\lambda)^{-1}$ for $s\in\mathbb{C}\backslash[0,1]$, $g(\lambda)\equiv 1$, $\vec{\xi}=\vec{e}_j$, and $\vec{\zeta}=\vec{e}_k$ in Equation (A.2), yields the integral formula for $F_{jk}(s)$ displayed in Equation (2.44), which is equivalent to that displayed in (2.12). It is now clear why the Hilbert space $\mathscr{H}_\times$ was extended to $\mathscr{H}_0$ in our formulation of the spectral theorem for the ACM: the appearance of the *constant* fields $\vec{e}_j$, $j=1,\ldots,d$, in Equation (2.44).

A.2. Finite lattice setting.   In this section, we review the spectral theorem as it pertains to the ACM for the finite lattice setting discussed in Section 2.2.2. In this case, the operator $M_1 = \chi_1\Gamma\chi_1$ is represented by a real-symmetric random matrix and the spectral theorem for such matrices provides a discrete version of the integral representation displayed in Equation (A.2). This formulation leads to the discrete integral representation of the function $F_{jk}(s)$ displayed in equations (2.36) and (2.44).

Recall that we defined in Section 2.2.2 a bijective mapping $\Theta: \mathbb{Z}_L^d \to \mathbb{N}_L$ from the finite d-dimensional bond lattice $\mathbb{Z}_L^d$ of size L onto the one-dimensional set $\mathbb{N}_L$ of size $N = dL^d$. Moreover, we showed that under the mapping Θ, the random operator $M_1 = \chi_1\Gamma\chi_1$ can be represented by a random matrix of size $N\times N$ [32, 58]. More specifically, Γ is a *non-random*, real-symmetric projection matrix satisfying $\Gamma^2=\Gamma$. Consequently, $\|\Gamma\|\leq 1$, where $\|\cdot\|$ denotes the matrix norm induced by the dot-product on $\mathbb{C}^N$ [23]. In this finite lattice setting, the characteristic function χ_1 is represented by a *random*, diagonal projection matrix satisfying $\chi_1^2=\chi_1$, with zeros and ones along its diagonal. Consequently, the matrix χ_1 is real-symmetric and satisfies $\|\chi_1\|\leq 1$.

It follows that M_1 is a real-symmetric composition of projection matrices with

$\|M_1\| \leq 1$ [23]. It is also a positive definite matrix, since for every $\vec{\xi} \in \mathbb{C}^N$ we have that $\chi_1 \Gamma \chi_1 \vec{\xi} \cdot \vec{\xi} = (\Gamma \chi_1 \vec{\xi}) \cdot (\Gamma \chi_1 \vec{\xi}) \geq 0$. This, in turn, implies that the spectrum Σ of M_1 is comprised of real eigenvalues λ_i, $i = 1, \ldots, N$, and that $\Sigma \subseteq [0, \infty)$ [44]. Furthermore, the largest eigenvalue of the matrix M_1 is equal to $\|M_1\|$ [23]. It follows that $\Sigma \subseteq [0, 1]$.

It is well known [44, 48] that the eigenvectors $\vec{u}_i$, $i = 1, \ldots, N$, of the real-symmetric matrix M_1 form an orthonormal basis for $\mathbb{R}^N$, i.e., $\vec{u}_\ell^T \vec{u}_m = \delta_{\ell m}$ and for every $\vec{\xi} \in \mathbb{R}^N$ we have $\vec{\xi} = \sum_{i=1}^N (\vec{u}_i^T \vec{\xi}) \vec{u}_i = \left(\sum_{i=1}^N \vec{u}_i \vec{u}_i^T \right) \vec{\xi}$. Consequently,

$$\sum_{i=1}^N Q_i = I, \qquad Q_i = \vec{u}_i \vec{u}_i^T, \qquad Q_\ell Q_m = Q_\ell \delta_{\ell m}, \tag{A.3}$$

where I is the identity matrix on $\mathbb{R}^N$. Here, we have defined Q_i, $i = 1, \ldots, N$, to be the mutually orthogonal projection matrices onto the eigenspaces spanned by the $\vec{u}_i$.

Since $M_1 \vec{u}_i = \lambda_i \vec{u}_i$, the identity $Q_i = \vec{u}_i \vec{u}_i^T$ implies that we also have $M_1 Q_i = \lambda_i Q_i$. This and Equation (A.3) then imply that the matrix M_1 has the spectral decomposition $M_1 = \sum_{i=1}^N \lambda_i Q_i$. By the mutual orthogonality of the projection matrices Q_i and by induction, we have that $M_1^n = \sum_{i=1}^N \lambda_i^n Q_i$ for all $n \in \mathbb{N}$. This, in turn, implies that $f(M_1) = \sum_{i=1}^N f(\lambda_i) Q_i$ for any polynomial $f : \mathbb{R} \mapsto \mathbb{C}$. In between equations (2.52) and (2.53) we argued that $\chi_1 Q_i = Q_i \chi_1 = \chi_1 Q_i \chi_1$, as $\chi_1 Q_i = 0$ for $i = 1, \ldots, N_0$ and $\chi_1 Q_i = Q_i$ otherwise. It now follows from Equation (A.3) that, for all $\vec{\xi}, \vec{\zeta} \in \mathbb{C}^N$ and complex valued polynomials $f(\lambda)$ and $g(\lambda)$, the bilinear functional $\langle f(M_1) \vec{\xi}, g(M_1) \vec{\zeta} \rangle_1 = \langle f(M_1) \chi_1 \vec{\xi} \cdot g(M_1) \vec{\zeta} \rangle$ has the following integral representation

$$\langle f(M_1) \vec{\xi}, g(M_1) \vec{\zeta} \rangle_1 = \int_0^1 f(\lambda) \bar{g}(\lambda) \mathrm{d}\mu_{\xi\zeta}(\lambda), \quad \mathrm{d}\mu_{\xi\zeta}(\lambda) = \sum_{i=1}^N \langle \delta_{\lambda_i}(\mathrm{d}\lambda) Q_i \vec{\xi} \cdot \vec{\zeta} \rangle_1. \tag{A.4}$$

The proof of Theorem 2.1 given in Section 2.2.4 demonstrates that Equation (A.4) also holds for the functions $f(\lambda) = (s - \lambda)^{-1}$ and $g(\lambda) \equiv 1$ when $s \in \mathbb{C} \backslash [0, 1]$. In this matrix setting, the projection valued operator $Q(\lambda)$ associated with the strictly increasing function $\mu_{\xi\zeta}(\lambda) = \langle Q(\lambda) \vec{\xi} \cdot \vec{\zeta} \rangle_1$ discussed in Section A.1 can be written explicitly as

$$Q(\lambda) = \sum_{i : \lambda_i < \lambda} \theta(\lambda - \lambda_i) Q_i. \tag{A.5}$$

Here, $\theta(\lambda)$ is the Heaviside function which takes the value $\theta(\lambda) = 0$ for $\lambda < 0$ and $\theta(\lambda) = 1$ for $\lambda > 0$.

REFERENCES

[1] N.I. Akhiezer, *The Classical Moment Problem*, Oliver & Boyd, 1965.

[2]   M. Avellaneda and A. Majda, *An integral representation and bounds on the effective diffusivity in passive advection by laminar and turbulent flows*, Commun. Math. Phys., 138, 339–391, 1991.

[3]   M. Avellaneda and M. Vergassola, *Stieltjes integral representation of effective diffusivities in time-dependent flows*, Phys. Rev. E, 52, 3249–3251, 1995.

[4]   L.G.E. Backstrom, *Capacitance Measurements of Bulk Salinity and Brine Movement in First-year Sea Ice*, University of Alaska Fairbanks, 2007.

[5]   S. Barabash and D. Stroud, *Spectral representation for the effective macroscopic response of a polycrystal: application to third-order non-linear susceptibility*, J. Phys., Condens. Matter, 11, 10323–10334, 1999.

[6]   D.J. Bergman, *The dielectric constant of a composite material – a problem in classical physics*, Phys. Rep. C, 43, 377–407, 1978.

[7]   D.J. Bergman, *Exactly solvable microscopic geometries and rigorous bounds for the complex dielectric constant of a two-component composite material*, Phys. Rev. Lett., 44, 1285–1287, 1980.

[8]   D.J. Bergman, *Rigorous bounds for the complex dielectric constant of a two–component composite*, Ann. Phys., 138, 78–114, 1982.

[9]   C. Bonifasi-Lista and E. Cherkaev, *Electrical impedance spectroscopy as a potential tool for recovering bone porosity*, Phys. Med. Biol., 54, 3063–3082, 2009.

[10] O. Bruno, *The effective conductivity of strongly heterogeneous composites*, Proc. R. Soc. London A, 433, 353–381, 1991.

[11] O. Bruno and K. Golden, *Interchangeability and bounds on the effective conductivity of the square lattice*, J. Stat. Phys., 61, 365–386, 1990.

[12] H. Cheng and L. Greengard, *On the numerical evaluation of electrostatic fields in dense random dispersions of cylinders*, J. Comput. Phys., 136, 629–639, 1997.

[13] E. Cherkaev, *Inverse homogenization for evaluation of effective properties of a mixture*, Inverse Problems, 17, 1203–1218, 2001.

[14] E. Cherkaev, *Spectral coupling of effective properties of a random mixture*, in IUTAM Symposium on Asymptotics, Singularities and Homogenisation in Problems of Mechanics, A.B. Movchan (ed.), Solid Mech. Appl., Springer Netherlands, 113, 331–340, 2004.

[15] E. Cherkaev and C. Bonifasi-Lista, *Characterization of structure and properties of bone by spectral measure method*, J. Biomech., 44, 345–351, 2011.

[16] E. Cherkaev and K.M. Golden, *Inverse bounds for microstructural parameters of composite media derived from complex permittivity measurements*, Waves in Random Media, 8, 437–450, 1998.

[17] E. Cherkaev and M.-J. Ou, *Dehomogenization: reconstruction of moments of the spectral measure of the composite*, Inverse Problems, 24, 065008, 2008.

[18] E. Cherkaev and D. Zhang, *Coupling of the effective properties of a random mixture through the reconstructed spectral representation*, Physica B: Condensed Matter, 338, 16–23, 2003.

[19] R.W.R. Darling, *Differential Forms and Connections*, Cambridge University Press, 1994.

[20] A.R. Day and M.F. Thorpe, *The spectral function of random resistor networks*, J. Phys., Condens. Matter, 8, 4389–4409, 1996.

[21] A.R. Day and M.F. Thorpe, *The spectral function of composites: the inverse problem*, J. Phys., Condens. Matter, 11, 2551–2568, 1999.

[22] P. Deift, *Orthogonal Polynomials and Random Matrices: A Riemann–Hilbert Approach*, Courant Institute of Mathematical Sciences, New York, NY, 2000.

[23] J.W. Demmel, *Applied Numerical Linear Algebra*, SIAM, 1997.

[24] N. Dunford and J.T. Schwartz, *Linear Operators, Part I*, John Wiley & Sons, Inc., Hoboken, NJ, 1988.

[25] R. Durrett, *Probability: Theory and Examples*, 4th Edition, Cambridge University Press, 2010.

[26] G.B. Folland, *Introduction to Partial Differential Equations*, Princeton University Press, Princeton, NJ, 1995.

[27] G.B. Folland, *Real Analysis: Modern Techniques and Their Applications*, Wiley–Interscience, New York, NY, 1999.

[28] K. Golden, *Bounds on the complex permittivity of a multicomponent material*, J. Mech. Phys. Solids, 34, 333–358, 1986.

[29] K.M. Golden, *Exponent inequalities for the bulk conductivity of a hierarchical model*, Commun. Math. Phys., 143, 467–499, 1992.

[30] K.M. Golden, *Critical behavior of transport in lattice and continuum percolation models*, Phys. Rev. Lett., 78, 3935–3938, 1997.

[31] K.M. Golden, *The interaction of microwaves with sea ice*, in Wave Propagation in Complex Media, IMA Volumes in Mathematics and its Applications, G. Papanicolaou (ed.), Springer – Verlag, 96, 75–94, 1997.

[32] K.M. Golden, N.B. Murphy, and E. Cherkaev, *Spectral analysis and connectivity of porous microstructures in bone*, J. Biomech., 44, 337–344, 2011.

[33] K.M. Golden and G. Papanicolaou, *Bounds for effective parameters of heterogeneous media by analytic continuation*, Commun. Math. Phys., 90, 473–491, 1983.

[34] K.M. Golden and G. Papanicolaou, *Bounds for effective parameters of multicomponent media by analytic continuation*, J. Stat. Phys., 40, 655–667, 1985.

[35] L. Greengard and J.-Y. Lee, *Electrostatics and heat conduction in high contrast composite materials*, J. Comput. Phys., 211, 64–76, 2006.

[36] L. Greengard and M. Moura, *On the numerical evaluation of electrostatic fields in composite materials*, Acta Numerica, 3, 379–410, 1994.

[37] A. Gully, J. Lin, E. Cherkaev, and K.M. Golden, *Bounds on the complex permittivity of polycrystalline materials by analytic continuation*, Proc. R. Soc. London A, 471, DOI: 10.1098/rspa.2014.0702, 2015.

[38] P.R. Halmos, *Finite Dimensional Vector Spaces*, Van Nostrand–Reinhold, Princeton, NJ, 1958.

[39] J. Helsing, *The effective conductivity of arrays of squares: Large random unit cells and extreme contrast ratios*, J. Comput. Phys., 230, 7533–7547, 2011.

[40] J. Helsing, *The effective conductivity of random checkerboards*, J. Comput. Phys., 230, 1171–1181, 2011.

[41] J. Helsing, R.C. McPhedran, and G.W. Milton, *Spectral super-resolution in metamaterial composites*, New J. Phys., 13, 115005, 2011.

[42] J. Helsing and R. Ojala, *Corner singularities for elliptic problems: Integral equations, graded meshes, quadrature, and compressed inverse preconditioning*, J. Comput. Phys., 227, 8820–8840, 2008.

[43] P. Henrici, *Applied and Computational Complex Analysis*, John Wiley & Sons Inc., New York, 2, 1974.

[44] R.A. Horn and C.R. Johnson, *Matrix Analysis*, Cambridge University Press, 1990.

[45] J.D. Jackson, *Classical Electrodynamics*, John Wiley and Sons, Inc., New York, 1999.

[46] T. Jonckheere and J.M. Luck, *Dielectric resonances of binary random networks*, J. Phys. A: Math. Gen., 31, 3687–3717, 1998.

[47] S. Karlin and W.J. Studden, *Tchebycheff Systems: with Applications in Analysis and Statistics*, John Wiley & Sons, Inc., Hoboken, NJ, 1966.

[48] J.P. Keener, *Principles of Applied Mathematics: Transformation and Approximation*, Westview Press, Cambridge, MA, 2000.

[49] J.B. Keller, *A theorem on the conductivity of a composite medium*, J. Math. Phys., 5, 548–549, 1964.

[50] D. McLaughlin, G. Papanicolaou, and O. Pironneau, *Convection of microstructure and related problems*, SIAM J. Appl. Math., 45, 780–797, 1985.

[51] R.C. McPhedran, D.R. McKenzie, and G.W. Milton, *Extraction of structural information from measured transport properties of composites*, Appl. Phys. A, 29, 19–27, 1982.

[52] R.C. McPhedran and G.W. Milton, *Inverse transport problems for composite media*, MRS Proceedings, 195, 1990.

[53] G.W. Milton, *Bounds on the complex dielectric constant of a composite material*, Appl. Phys. Lett., 37, 300–302, 1980.

[54] G.W. Milton, *Bounds on the complex permittivity of a two component composite material*, J. Appl. Phys., 52, 5286–5293, 1981.

[55] G.W. Milton, *Bounds on the transport and optical properties of a two-component composite material*, J. Appl. Phys., 52, 5294–5304, 1981.

[56] G.W. Milton, *Theory of Composites*, Cambridge University Press, Cambridge, 2002.

[57] N.B. Murphy, *Phase transitions in random media*, PhD thesis, University of Utah, 2012.

[58] N.B. Murphy and K.M. Golden, *The Ising model and critical behavior of transport in binary composite media*, J. Math. Phys., 53, 063506(1–25), 2012.

[59] C. Orum, E. Cherkaev, and K.M. Golden, *Recovery of inclusion separations in strongly heterogeneous composites from effective property measurements*, Proc. R. Soc. London A, 468, 784–809, 2012.

[60] M.J. Ou and E. Cherkaev, *On the integral representation formula for a two-component elastic composite*, Math. Meth. Appl. Sci., 29, 655–664, 2006.

[61] M.Y. Ou, *Two-parameter integral representation formula for the effective elastic moduli of two-phase composites*, Complex Var. Elliptic Equ., 57, 411–424, 2012.

[62] G. Papanicolaou and S. Varadhan, *Boundary value problems with rapidly oscillating coefficients*, in Colloquia Mathematica Societatis János Bolyai 27, Random Fields (Esztergom, Hungary 1979), North-Holland, 835–873, 1982.

[63] M.C. Reed and B. Simon, *Functional Analysis*, Academic Press, San Diego CA, 1980.

[64] W. Rudin, *Real and Complex Analysis*, McGraw-Hill, Inc., New York, NY, 1987.

[65] B.K.P. Scaife, *Principles of Dielectrics*, Clarendon Press, Oxford, 1989.

[66] K. Schulgasser, *On the conductivity of fiber reinforced materials*, J. Math. Phys., 17, 382–387, 1976.

[67] J.A. Shohat and J.D. Tamarkin, *The Problem of Moments*, American Mathematical Society, Providence, RI, 1963.

[68] L.B. Simeonova, D.C. Dobson, O. Eso, and K.M. Golden, *Spatial bounds on the effective complex permittivity for time-harmonic waves in random media*, Multiscale Modeling and Simulation, 9, 1113–1143, 2011.

[69] I. Stakgold, *Boundary Value Problems of Mathematical Physics: 2-Volume Set*, Classics in Applied Mathematics, SIAM, 2000.

[70] D. Stauffer and A. Aharony, *Introduction to Percolation Theory*, Taylor and Francis, London, 2nd Edition, 1992.

[71] T.-J. Stieltjes, *Recherches sur les fractions continues*, Ann. Fac. Sci. Toulouse Math., 4, J1–J35, 1995.

[72] M.H. Stone, *Linear Transformations in Hilbert Space*, American Mathematical Society, Providence, RI, 1964.

[73] S. Torquato, *Random Heterogeneous Materials: Microstructure and Macroscopic Properties*, Springer-Verlag, New York, 2002.

[74] L. Trefethen and D. Bau, *Numerical Linear Algebra*, Society for Industrial and Applied Mathematics, 1997.

[75] D. Zhang and E. Cherkaev, *Reconstruction of spectral function from effective permittivity of a composite material using rational function approximations*, J. Comput. Phys., 228, 5390–5409, 2009.